ARMY RESEARCH LABORATORY

A Prototype Acoustic Battlefield Decision Aid Incorporating Atmospheric Effects and Arbitrary Sensor Layouts

by D. Keith Wilson

ARL-TR-1708 September 1998

The findings in this report are not to be construed as an official Department of the Army position unless so designated by other authorized documents.

Citation of manufacturer's or trade names does not constitute an official endorsement or approval of the use thereof.

Destroy this report when it is no longer needed. Do not return it to the originator.

Army Research Laboratory
Adelphi, MD 20783-1197

ARL-TR-1708 **September 1998**

A Prototype Acoustic Battlefield Decision Aid Incorporating Atmospheric Effects and Arbitrary Sensor Layouts

D. Keith Wilson
Information Science and Technology Directorate

Abstract

The Acoustic Battlefield Aid (ABFA) is a prototype decision aid for assessing the performance of acoustic sensors in different environments. ABFA combines accurate modeling of atmospheric effects on acoustic signals with newly developed methods for determining acoustic array performance. The report describes the methods by which ABFA calculates such quantities as transmission loss, signal-to-noise ratio, detection probability, array direction-finding accuracy, and position-finding accuracy from array networks. Some example calculations are provided for propagation over rough terrain in various weather conditions.

Contents

Figures

Tables

1. Introduction

Acoustical systems can be used to detect, locate, and classify targets on the battlefield. They offer many potential benefits for such uses: low cost, ruggedness, versatility, passive operation, and detection capability in non-line-of-sight situations. They also provide information that can complement existing optical and infrared technologies. Thus it appears that acoustical systems will play a valuable role on the future battlefield.

One important characteristic of acoustical systems, which must be accounted for in battlefield applications, is that their performance depends heavily on atmospheric conditions and the local terrain. The atmosphere and terrain alter the acoustic signal as it propagates from the source to the sensor. Some important propagation effects are illustrated in figure 1. Unfortunately, few practical tools have as yet been available that can take these propagation effects into account. This report describes a prototype decision aid, called the *Acoustic Battlefield Aid* (ABFA), which has been designed to remedy this shortcoming.

In its current form, ABFA is best described as a demonstration model. Developed by the U.S. Army Research Laboratory (ARL), ABFA provides

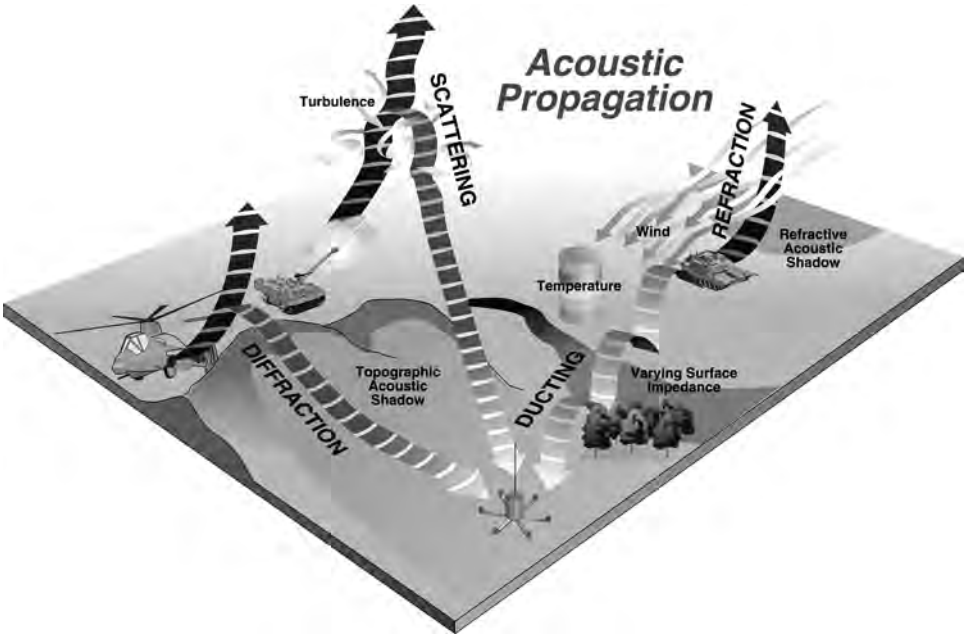

Figure 1. Influences of atmosphere and terrain on sound propagation.

a new conceptual framework for how an acoustical tactical decision aid can be designed and implemented. Work must still be done to verify its predictions, and to refine it so that it is useful in Army applications. It is hoped that the general design and underlying methodologies of ABFA will help lead future development of useful, flexible, and reliable tools for characterizing acoustic sensor performance.

ABFA incorporates recent scientific and technological advances for predicting acoustic propagation, and for characterizing sensor array performance in the randomly varying (turbulent) atmosphere. Several state-of-the-art research products are merged into a simple, graphical user interface. The acoustical algorithms have been carefully implemented to characterize sensor performance in a computationally efficient, yet reliable, manner.

The emphasis of this report is on the various algorithms used for ABFA's calculations. It is not intended as a user's guide, nor as a discussion of the performance of actual sensor systems. These matters (although of course important) are beyond the scope of this report.

The report begins with a discussion of some of the broad conceptual issues relevant to the design of ABFA (sect. 2). I then discuss ABFA's method for handling different types of sources and receivers (sect. 3), atmospheric modeling (sect. 4), and terrain modeling (sect. 5). The acoustic propagation models incorporated into ABFA are discussed in section 6, and the methods by which sensor performance is quantified in section 7. Section 8 provides some example calculations.

The report has been organized so that readers who are interested mainly in the capabilities of ABFA, rather than in the technical details of its underlying algorithms, can skip directly to the examples in section 8.

2. The General Design of ABFA

ABFA is ambitious in scope: it attempts to seamlessly incorporate atmospheric and terrain characterization, the properties of different acoustic sources and receivers, several acoustic propagation models, and statistical methods for determining the effects of random atmospheric fluctuations (turbulence) on the information yielded by the sensors. In order to achieve this goal, ABFA makes certain reasonable sacrifices regarding the exactness of the calculations. This is necessary because exact characterization of the performance of a given sensor requires mimicking the sensor's electronics, its data processing algorithms, and the complicated interactions between the sensor and and its environment. Accounting for all these aspects of the problem would be a prohibitively complex and computationally infeasible endeavor for a multipurpose tool such as ABFA. Furthermore, such exactitude would involve classified details of a sensor's design and operation. Hence there is a strong motivation to decide which features of the combined acoustic propagation/sensor scenario most significantly affect the sensor performance, and to model these according to general principles. The following are some of the general modeling principles implicit in ABFA, and their corresponding rationales:

- *Principle:* Characterization of the acoustic sensor performance must account for the influence of atmospheric conditions and terrain on signal propagation.

  Rationale: Sound levels are dramatically affected by refraction and diffraction by atmospheric wind and temperature gradients, and by shadows created by terrain. Atmospheric winds also produce noise on microphones that is often the limiting factor in low-frequency detection capability. For propagation distances more than a few hundred meters, acoustic sensor performance depends so heavily on atmospheric conditions and terrain that a decision aid not incorporating them is nearly useless.

- *Principle:* Sensor performance should be characterized by metrics that are broadly applicable to well-designed sensors, rather than by an attempt to mimic the specific electronics and data processing algorithms of the sensor.

Rationale: Signal processing algorithms used by acoustic sensor systems vary widely and are often quite complicated. Furthermore, mimicking most good processing algorithms would impose an impractical computational burden on the propagation model. Fortunately, there are well-established methods for approximating the performance obtainable by a well-designed sensor and processing algorithm. The metric used by ABFA is called the *Cramer-Rao lower bound* (CRLB), which describes the performance of an optimal sensor. The CRLB is fairly easy to calculate, and previous studies have shown that good processing algorithms attain performance comparable to the CRLB (Song and Ritcey, 1996).

- *Principle:* The decision aid should interface simply with a variety of data sources for the atmospheric and terrain inputs.

  Rationale: The decision aid may be used in scenarios ranging from simulations to actual implementation on the battlefield. It should interface sensibly with available data sources, regardless of the quality and resolution of the input. The current version of ABFA is configured to accept new data formats without changes to the functionality.

- *Principle:* The decision aid should be a flexible, multipurpose tool, incorporating calculations and displays of such diverse quantities as transmission loss, signal-to-noise ratio (SNR), detection probabilities, accuracy of sensor arrays for determining target bearings, and accuracy of multiple array configurations for locating targets.

  Rationale: The most difficult part of the acoustical calculation is the effect of atmospheric conditions and terrain on the acoustic propagation. Other types of plots are basically enhancements of the propagation information, with some small additional processing. Therefore there is little reason for making separate decision aids for different display purposes.

With regard to the last principle, the main effect of the weather and terrain is to alter the transmission loss (also called the *propagation loss*) from the source to the receiver. Calculation of the transmission loss is the first step in all ABFA calculations. Once the transmission loss is known, the SNR can be calculated from the source and background noise levels. Other calculations, involving array performance, follow from the SNR. The basic hierarchy in calculations made by ABFA, and the inputs at each step, are shown in figure 2. Results of any of the intermediate calculations are available for plotting.

ABFA was programmed in the high-level Matlab language. The built-in matrix routines, graphical capabilities, and GUI (graphical user interface) functions of Matlab made it possible to produce ABFA with limited programming effort. The initial screen presented to the user is shown in figure 3.

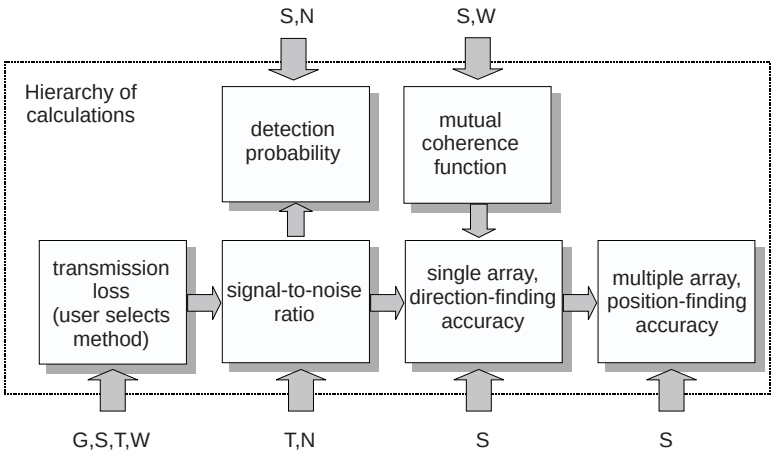

Figure 2. Hierarchy of calculations available from ABFA. Inputs: G = ground and terrain; N = background noise; S = sensor (receiver); T = target (source); and W = weather (atmospheric characterization).

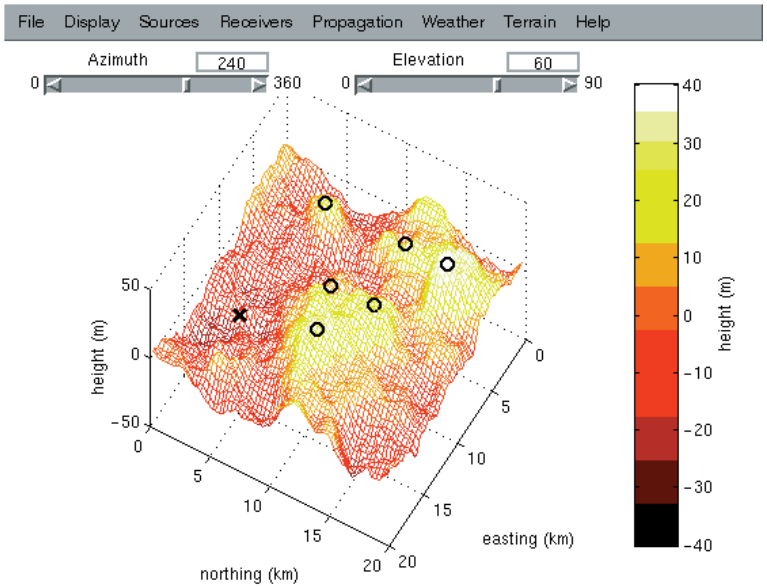

Figure 3. ABFA's graphical user interface. This initial screen shows topography and all source (×) and receiver (◯) locations. Alternative displays, such as signal-to-noise ratio and probability of detection, are selected from "Display" menu.

The drawback of using Matlab to create ABFA is, of course, that the Matlab interpreter must be available to run the program. Current ARL projects include the creation of an attractive GUI, written in the C++ language, for running acoustical prediction models. Plans include conversion of many of ABFA's algorithms to C++. With regard to these plans, it is worth pointing out that The MathWorks, Inc. (makers of Matlab), recently introduced a compiler that converts Matlab code to C. However, routines with graphics commands cannot be compiled. Therefore only the computational parts of the code can be converted to C with the Matlab compiler.

3. Source and Receiver Models

As discussed above, one of the guiding principles in the design of ABFA was that it should *estimate* the performance of a *well-designed sensor*, rather than predicting precisely how a particular sensor system will operate. The decision to design ABFA in this manner is, of course, a compromise: it would be ideal if the performance of a given sensor could be simulated precisely, but practical considerations often prevent this.

In ABFA, each source is assumed to be omnidirectional and is represented by a single characteristic frequency f_c and a finite bandwidth Δf. The characteristic frequency is taken to be the geometric mean of the lower (f_ℓ) and upper (f_u) frequencies in the band:

$$\begin{aligned} f_c &= \sqrt{f_\ell f_u}, \\ \Delta f &= f_u - f_\ell. \end{aligned}$$

To calculate the signal transmission loss (the difference between the signal amplitude at a distance of 1 m from the source,* and its level at the receiver), the frequency f_c is used. The source is essentially modeled as a harmonic point source for this part of the computation. But for calculating the SNR, all the noise energy in the band $[f_\ell, f_u]$ is summed to produce the total noise background.

The reason for using a single frequency and bandwidth to model sources is to save computational time. Most of the computational time in an ABFA calculation is usually spent in the propagation model, which must be run separately for each frequency. Hence the single-frequency method minimizes computational time.

It should be made clear that, even though ABFA runs the propagation model at just one frequency, there is no implication that the actual source emits acoustic waves just at that single frequency. What is implied is that the propagation characteristics of that single frequency are *representative* of propagation for the frequency band (or set of frequencies) used by a particular sensor. For example, suppose a tank is modeled as a source having center frequency f_c = 100 Hz and bandwidth Δf = 150 Hz (f_ℓ = 50 Hz, f_u = 200 Hz). Further suppose that a particular sensor and

*The reference distance of 1 m from the source is an accepted standard in acoustics research and noise control applications.

processing algorithm uses information from frequency lines such as 80, 100, and 150 Hz. Since the transmission losses at these three frequencies are normally similar to those at 100 Hz, the ABFA prediction should work reasonably well. On the other hand, if information at a very low frequency (such as 20 Hz) is used by the sensor, the ABFA propagation calculation may not be satisfactorily representative. Furthermore, contributions from wind noise below f_ℓ = 50 Hz would be neglected, which may be quite significant in high-wind conditions.

The single-frequency method used by ABFA is just a convenient (and usually reasonable) assumption used to create the prototype. Eventually it may be desirable to upgrade ABFA from its present form to one that models the performance of specific sensor systems with higher accuracy, in which case the single representative frequency method can easily be upgraded to incorporate several representative frequencies.

In the current version of ABFA, receivers consist of ideal point microphones having flat (frequency-independent) responses. For most microphone types and acoustic frequencies of interest, the assumptions of a point receiver and a flat response are quite reasonable. The microphones may be arranged in coherent-processing arrays having a linear, circular, or triangular geometry. In all these cases, the number of elements and the spacing are chosen by the user.

The microphones are assumed to be equipped with 9-cm-diameter windscreens. The effect of the windscreen is accounted for in the SNR calculation (sect. 7.1). Arbitrarily sized windscreens may be incorporated into a future version of ABFA.

4. Atmospheric Models

When the wind and temperature vary with height, sound energy is refracted, a process that tremendously influences sound levels in the atmosphere. ABFA provides three basic methods for entering the mean wind and temperature profiles used for the calculations. The first of these involves user selection from a half-dozen "typical" cases, described in detail by Noble (1994). The second method, called *Monin-Obukhov* (MO) *similarity scaling,* is based on a statistical parameterization for atmospheric turbulence that has been well verified during the past several decades. MO-similarity is described in section 4.1. The third method is simply to load a file containing arbitrary profiles. This method is useful if data are available from a radiosonde or other meteorological instrumentation.

ABFA's calculations involving arrays require statistical information on the turbulent fluctuations of wind and temperature, in addition to the plain mean profiles. The turbulent fluctuations are parameterized with structure functions, as described in section 4.2.

4.1 Monin-Obukhov Similarity Modeling

The wind and temperature profiles in the atmospheric surface layer (the 10 to 200 m nearest the ground) are determined by turbulent mixing. Although it is not generally possible to solve problems involving turbulent mixing on the basis of first principles, there are scaling methods that have been found to yield reliable results. For the atmospheric surface layer profiles, the MO-similarity (Panofsky and Dutton, 1984; Stull, 1988) scaling method is often used.

MO-similarity is based on the premise that atmospheric turbulence structure near the ground depends entirely on four quantities: the height z, the stress τ exerted by the wind on the ground, the surface heat flux Q, and the buoyancy $\beta = g/\theta_0$, where g is gravitational acceleration and θ_0 is the surface temperature. From these four quantities, representative scales for length, velocity, and temperature can be formulated.

The velocity scale, called the *friction velocity*, is

$$u_* = \sqrt{\frac{\tau}{\rho}}, \tag{1}$$

where ρ is the density of air. The *surface-layer temperature scale* is

$$T_* = -\frac{Q}{u_*}. \tag{2}$$

Last, the length scale, called the *Monin-Obukhov length*, is

$$L_{mo} = -\frac{u_*^3}{\kappa\beta Q}, \tag{3}$$

where $\kappa = 0.4$ is called von Kármán's constant.

According to MO-similarity, the mean profiles must be universal functions of the ratio $\zeta = z/L_{mo}$. As a result, the profiles for the mean wind speed and temperature can be written

$$u(z) = \frac{u_*}{\kappa}\left[\ln\frac{z}{z_0} - \Psi_M\left(\frac{z}{L_{mo}}\right) + \Psi_M\left(\frac{z}{L_{mo}}\right)\right], \quad \text{and} \tag{4}$$

$$T(z) = T(z_{ref}) + \frac{T_* P_t}{\kappa}\left[\ln\frac{z}{z_{ref}} - \Psi_H\left(\frac{z}{L_{mo}}\right) + \Psi_H\left(\frac{z_{ref}}{L_{mo}}\right)\right], \tag{5}$$

where z_0 is called the roughness height (height where the mean wind vanishes), z_{ref} is some reference height at which the temperature is known, $P_t \simeq 0.74$, Ψ_M is the universal profile function for momentum, and Ψ_H is the universal profile function for heat. For the universal functions, ABFA uses the forms proposed by Carl *et al* (1973; see also L'Espérance *et al*, 1993):

$$\Psi_M(\zeta) = \Psi_H(\zeta) = \frac{3}{2}\ln\frac{1-\phi^{-1}+\phi^{-2}}{3} + \sqrt{3}\tan^{-1}\frac{2\phi+1}{\sqrt{3}}, \quad \zeta < 0,$$
$$\Psi_M(\zeta) = \Psi_H(\zeta)/P_t = -4.7\zeta, \quad \zeta > 0,$$

where

$$\phi_M(\zeta) = (1-15\zeta)^{-1/3},$$
$$\phi_H(\zeta) = (1-9\zeta)^{-1/3}.$$

Sometimes, particularly when conditions are very sunny and the wind very light, MO-similarity is known to break down. The reason is that large, boundary-layer-size eddies (typically 1 to 2 km in size) begin to play an important role in turbulent mixing even very near the ground. In these cases, instead of using the scaling parameters described above, one should switch to the convective boundary-layer scaling parameters (Stull, 1988)

$$w_* = (Q\beta z_i)^{1/3},$$
$$\theta_* = -\frac{Q}{w_*}.$$

These scales are for velocity and temperature, respectively. The appropriate length scale is z_i, the height of the boundary-layer inversion. In situations where turbulent structure depends primarily on free convection, ABFA automatically switches from MO-similarity to convective scaling.

ABFA allows the user to enter arbitrary values for u_*, T_*, and z_i. Alternatively, the user can select a set of values based on a subjective description of the weather conditions. Table 1 shows the different weather conditions available, and the corresponding values of u_*, T_*, and z_i.

4.2 Structure-Function Parameters

Structure-function parameters are useful for characterizing the "strength" of turbulence. They appear in statistical descriptions of wave propagation when scattering by eddies in the inertial subrange is analyzed. (The inertial subrange in the atmosphere generally consists of eddies smaller than the height from the ground, and larger than 1 mm.) The structure-function parameters are given by the equations

$$\begin{aligned} C_V^2 &= 2\epsilon^{2/3}, \\ C_T^2 &= 3\chi\epsilon^{-1/3} \end{aligned}$$

(as given in Stull, 1998, and elsewhere), where the dissipation rate for turbulent kinetic energy is

$$\epsilon \simeq \max\left(\frac{u_*^3}{0.4z}, \frac{w_*^3}{z_i}\right),$$

and the destruction rate for temperature variance is

$$\chi \simeq 0.43\frac{w_*\theta_*^2}{z_i}\left(\frac{z}{z_i}\right)^{-4/3}.$$

Table 1. Preselected meteorological conditions, based on Monin-Obukhov similarity scaling, available in ABFA.

Description	u_* (m/s)	T_* (K)	z_i (m)
mostly sunny and calm	0.1	-0.3	1000
mostly sunny and windy	0.5	-0.1	1000
clear night and calm	0.1	0.02	100
clear night and windy	0.5	0.05	100
overcast (day or night) and calm	0.1	-0.01	1000
overcast (day or night) and windy	0.5	-0.01	1000

5. Terrain Models

ABFA provides two basic options for generating topography (elevation models) in the simulation. One of these is simply to load a file that contains a two-dimensional array whose elements correspond to heights at evenly spaced, rectangular grid points. For the other option—generating a random terrain based on a height spectrum—ABFA provides two spectra: Gaussian and von Kármán. The method of generating the synthetic terrain is essentially the same for either model. First, a power spectrum for the heights is used to determine the strength of the Fourier (wavenumber-domain) modes. Each Fourier component is then multiplied by a random phase. Finally, an inverse Fourier transform is applied to produce the spatial-domain terrain. This section describes the two prescribed spectra, along with the selections available for small-scale terrain roughness features, such as grass and trees.

5.1 Gaussian Spectrum

The Gaussian model uses the following power spectrum:

$$S(k) = \frac{\sigma^2 L^2}{2} \exp\left(-\frac{k^2 L^2}{4}\right), \tag{6}$$

where k is the radial wavenumber ($k^2 = k_x^2 + k_y^2$), σ^2 is the variance in the terrain height, and L is the length scale of the terrain features. The Gaussian model yields terrain having a smooth appearance, with the "hills" all having horizontal dimensions comparable to L.

5.2 Von Kármán Spectrum

The von Kármán model is based on the following equation for the power spectrum, which is similar to one commonly used to describe turbulence:

$$S(k) = \frac{\sigma^2 L^2 \nu}{2\pi} \left(1 + k^2 L^2\right)^{-1-\nu}. \tag{7}$$

Here the parameter ν is called the *spectral roll-off parameter*. Like the Gaussian model, the von Kármán model produces terrain with strong features having length scales comparable to L. The main difference

between the models is that the von Kármán model also contains noticeable features having scales smaller than L, resulting in a realistic, rough appearance to the terrain not evident in the Gaussian model. The amount of roughness can be controlled by adjustments to ν, which is related to the fractal dimension of the terrain. Higher values of ν correspond to more roughness and higher fractal dimension.

5.3 Surface Roughness Characterization

Besides the actual changes in terrain elevation, it is important to have some characterization of the ground surface and the small-scale aerodynamic features existing on the terrain (e.g., desert, forest, urban). In the terminology of fluid dynamics, these features are called the *roughness elements*. They determine the roughness length z_0 used in the wind profile, equation (4). ABFA provides a set of choices for the terrain ground type, each having a characteristic roughness. The terrain types and corresponding roughness lengths are shown in table 2. The roughness lengths were adapted from Panofsky and Dutton's (1984) table 6.2.

Table 2. Selections for terrain type and corresponding values for surface roughness length z_0.

Description	Roughness length z_0 (m)
asphalt or ice	10^{-4}
open water	10^{-3}
snow	2×10^{-3}
desert (sand)	10^{-2}
short grass	10^{-2}
long grass or crops	5×10^{-2}
brush	0.1
suburban	0.4
forest	1
city	10

6. Propagation Models

Calculations of sensor array performance depend on knowledge of the signal-to-noise ratio (SNR) and the signal coherence between the sensors in the array. In order to find the SNR, one needs to know the reduction in signal level due to propagation between the source and the receiver. When expressed in decibels, this reduction is called the *transmission loss* (TL). It is defined by

$$\mathrm{TL} = 20 \log S - 20 \log_{10} |p(\mathbf{R})|, \tag{8}$$

where $p(\mathbf{R})$ is the complex acoustic pressure at the location $\mathbf{R}$, and S is the strength of the source measured in free space at 1 m. (By definition, the TL of a source radiating into free space, measured at a distance 1 m, is 0 dB.)

ABFA contains five models (four distinct and one hybrid) for determining TL. These are discussed in sections 6.1 to 6.5, in order of increasing complexity. The signal coherence between the sensors is quantified via the mutual coherence function (MCF), which is discussed in section 6.6.

6.1 Hard Surface Model

The sound field above a perfectly reflecting (hard) surface can be written as the sum of a contribution traveling directly from the source and one reflecting from the surface. The surface reflection can be thought of as emanating from an image source at a height $-z_s$, where z_s is the height of the actual source, as shown in figure 4. The acoustic pressure field generated by a single, unit-strength source is

$$G(R) = \frac{\exp(ikR)}{R}, \tag{9}$$

where k is the wavenumber, and R is the distance between the source and receiver. The function $G(R)$ is called the *free-space Green's function*. When the contributions from the real and image sources are summed and then multiplied by the source strength, we arrive at the following equation for the total pressure field:

$$p = S[G(R) + G(R_i)], \tag{10}$$

where

$$\begin{aligned} R^2 &= (x - x_s)^2 + (y - y_s)^2 + (z - z_s)^2, \\ R_i^2 &= (x - x_s)^2 + (y - y_s)^2 + (z + z_s)^2. \end{aligned}$$

Figure 4. A source above a hard boundary, showing resulting image source.

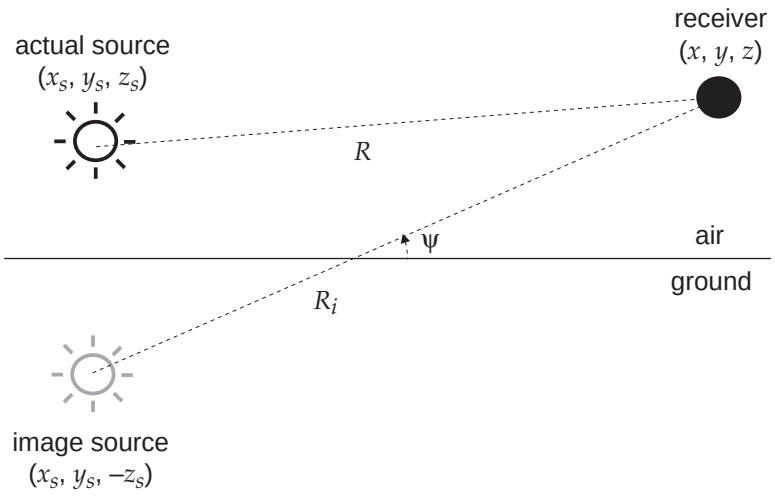

6.2 Impedance Ground Model

The hard-surface model discussed in the previous section assumes that all the sound energy incident on the ground plane is reflected. In actuality, the ground absorbs some fraction of the sound energy. We can account for this partial absorption by modeling the ground as a finite impedance surface. A perfectly hard surface corresponds to an infinite impedance.

Chien and Soroka (1975) have previously determined the sound field above a locally reacting, finite-impedance surface. Their solution has a form very similar to the hard-surface case:

$$p = S\left[G\left(R\right) + Q\left(\psi, w\right) G\left(R_i\right)\right], \tag{11}$$

where $Q\left(\psi, w\right)$ modifies the strength of the reflection. The angle ψ is defined in figure 4, and the quantity w is given by

$$w^2 = \frac{ikR_i}{2}\left(\sin\psi + \frac{\rho_0 c_0}{Z_s}\right)^2, \tag{12}$$

where ρ_0 is the air density, c_0 the sound speed in the air, and Z_s the surface impedance. The function $Q\left(\psi, w\right)$ is written

$$Q\left(\psi, w\right) = R\left(\psi\right) + \left[1 - R\left(\psi\right)\right] F\left(w\right), \tag{13}$$

in which

$$R\left(\psi\right) = \frac{\sin\psi - \rho_0 c_0 / Z_s}{\sin\psi + \rho_0 c_0 / Z_s} \tag{14}$$

is called the plane-wave reflection coefficient, and

$$F\left(w\right) = 1 + i\sqrt{\pi} w \exp\left(-w^2\right) \operatorname{erfc}\left(-iw\right). \tag{15}$$

ABFA determines the surface impedance using a Biot/Allard-like, porous, relaxational model (Wilson, 1997b). There are four parameters in the model: the static flow resistivity σ, the tortuosity q, the porosity Ω, and the Biot/Allard shape factor s_B. Values for these parameters are set based on the terrain ground type (sect. 5.3), and are given in table 3. These values are representative of the measurements described by Embleton *et al.* (1983), Martens *et al.* (1985), and Attenborough and Buser (1988).

Table 3. Ground parameters used in relaxational model. Water and ice cases both use an infinite surface impedance.

Description	σ (Pa · s/m^2)	q^2	Ω (%)	s_B
asphalt, city	3×10^7	3.2	10	1
open water or ice	infinite	—	—	—
snow	10^4	1.7	60	1
desert (sand)	4×10^5	1.6	40	1
grass (short or long), crops, brush, suburban	2×10^5	1.4	50	1
forest	10^5	1.3	60	1

6.3 Wedge Diffraction Model

The propagation models discussed so far have neglected terrain features such as hills and valleys. Although there are no exact, analytical solutions for the sound field over arbitrary terrain features, solutions have been calculated for some idealized surface geometries. One such geometry that has a tractable solution is the wedge shape, shown in figure 5. The angle β in figure 5 is called the *exterior wedge angle*, and $\nu = \pi/\beta$ ($\geq 1/2$) is called the *wedge index*.

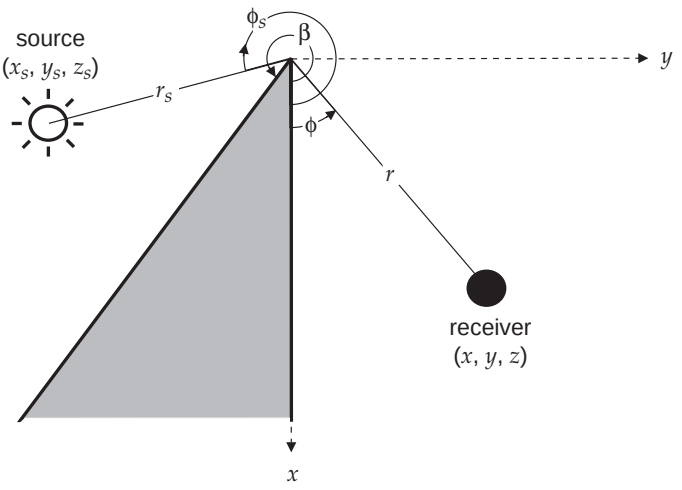

Figure 5. Geometry for propagation around a wedge. Shown is a cross section through wedge; it is actually infinite along axis perpendicular to page (z-axis).

The form of the solution for the wave field around a wedge that is incorporated into ABFA is due to Pierce (1981). The total pressure field is decomposed into two contributions, one part from *geometrical acoustics* and the other from *diffraction*:

$$p = p_{GA} + p_D.$$

One can obtain Pierce's form of the geometrical acoustics solution by writing the Green's function for a point source in a slightly different form. First note from figure 5 and the law of cosines that

$$R^2 = r^2 + r_s^2 - 2rr_s\cos\zeta + (z - z_s)^2,$$

where $\zeta = \phi - \phi_s$ is the angle between the source and receiver. Let us now write the Green's function in terms of dependence on ζ instead of dependence on R:

$$\mathcal{G}(\zeta) = G(R) = \frac{\exp\left(ik\sqrt{r^2 + r_s^2 - 2rr_s\cos\zeta + (z - z_s)^2}\right)}{\sqrt{r^2 + r_s^2 - 2rr_s\cos\zeta + (z - z_s)^2}}. \tag{16}$$

Using this form of the Green's function, we find that the geometric acoustics component of the solution is (Pierce's equation (9-8.1))

$$p_{GA} = S\left[\sum_n \mathcal{G}(2\beta n - \phi + \phi_s) + \sum_n \mathcal{G}(2\beta n - \phi - \phi_s)\right], \tag{17}$$

where the summation extends over all values for which the argument of the Green's function is between $-\pi$ and π. It is straightforward to show that equation (17) reduces to (10) when $\beta = \pi$.

The equation used by ABFA for the diffracted contribution is an asymptotic expression valid for $kr \gg 1$ and $kr_s \gg 1$, given by Pierce as equations (9-8.10) and (9-8.11):

$$p_D = S\frac{\exp(ikL - i\pi/4)\sin\nu\pi}{\sqrt{2}L}\left[\frac{A_D(\Gamma M_\nu(\phi - \phi_s))}{1 - \cos\nu\pi\cos\nu(\phi - \phi_s)} + \frac{A_D(\Gamma M_\nu(\phi + \phi_s))}{1 - \cos\nu\pi\cos\nu(\phi + \phi_s)}\right], \tag{18}$$

where

$$A_D(X) = \operatorname{sign}(X)\left[f(|X|) - ig(|X|)\right], \tag{19}$$

$$M_\nu(\phi) = \frac{\cos\nu\pi - \cos\nu\phi}{\nu\left(1 - \cos\nu\pi\cos\nu\phi\right)^{1/2}}, \tag{20}$$

$$\Gamma^2 = \frac{krr_s}{\pi L}, \quad \text{and} \tag{21}$$

$$L^2 = (r + r_s)^2 + z^2. \tag{22}$$

The functions f and g are called the *Fresnel auxiliary functions*, and are given approximately by (Abramowitz and Stegun, 1965, eq (7.3.32) and (7.3.33))

$$f(x) = \frac{1 + 0.926x}{2 + 1.792x + 3.104x^2}, \quad \text{and}$$
$$g(x) = \frac{1}{2 + 4.142x + 3.492x^2 + 6.670x^3}.$$

ABFA provides a propagation model option called the "wedge model." The wedge model, as the name suggests, is based on the solution for the field around a wedge given above. Given source and receiver locations, the intervening topographical features are approximated by a single wedge. The point of the wedge corresponds to the high point (apex) of the intervening terrain, as shown in figure 6. Note that the propagation coordinates used by ABFA (x and y horizontal, and z vertical) are different from the coordinate system used in figure 5. It is a simple matter, however, to shift the propagation coordinates so that the point of the wedge corresponds to the origin, and then rotate them to agree with figure 5.

6.4 Fast Field Program

The fast field program (FFP) is a method for computing sound fields in horizontally stratified environments, and hence can be used to calculate refraction by vertical gradients of wind and temperature. Originally developed for ocean acoustics, the FFP was first used for atmospheric propagation over a decade ago (Raspet *et al.*, 1985). The FFP formulation incorporated into ABFA is described elsewhere (Wilson, 1993).

The FFP is an excellent tool for determining meteorological effects on sound propagation. Unlike such methods as ray tracing, the FFP works well at low frequency and in refractive shadow regions. Unfortunately, since it is limited to horizontally stratified environments, the FFP is applicable only to propagation over flat ground. Therefore the FFP can give good results only in situations where the terrain is nearly flat.

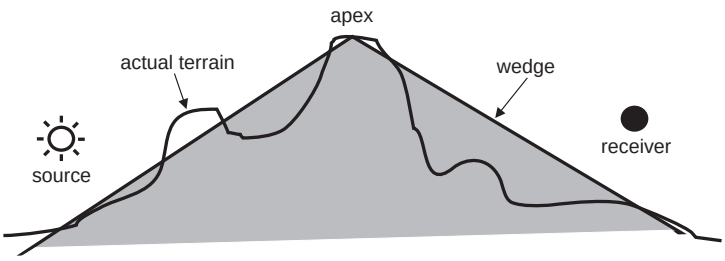

Figure 6. Approximation of rough terrain by a wedge shape.

The FFP in ABFA uses the meteorological models discussed earlier (sect. 4). The program automatically selects the resolution of the calculation in a manner that is appropriate for the dimensions of the simulated grid. The ground is modeled as a porous half space, with parameters given by table 3 (p 16).

6.5 Hybrid Wedge Models

In order to handle situations where *both* terrain and atmospheric effects are important, ABFA contains a hybrid propagation model that uses both the wedge and FFP calculations. The hybrid model is reasonably fast, but not as rigorous as the pure wedge or FFP models. The hybrid model calculates the transmission losses corresponding to the hard, flat surface (TL_H), the wedge (TL_W), and the FFP (TL_{FFP}), and then combines them incoherently:

$$\mathrm{TL}_{total} = \mathrm{TL}_{FFP} + \mathrm{TL}_W - \mathrm{TL}_H. \tag{23}$$

Note that the transmission losses for the wedge and FFP are added together, and then the TL for the hard surface is subtracted. The rationale behind this approach is that both the wedge and FFP calculations already include the effect of spherical spreading over a ground surface. Therefore the hard-surface contribution from the wedge model needs to be subtracted from the overall solution. The remaining propagation effects are then, in essence, simply summed together in decibels. These effects include terrain (from the wedge model), meteorological effects (from the FFP), ground impedance effects (from the FFP), and atmospheric absorption (from the FFP).

ABFA also incorporates a hybrid wedge/impedance ground model option for convenience. The equation for this model is the same as equation (23), although with TL_{GI} (the TL from the impedance ground model) replacing TL_{FFP}. The hybrid wedge/impedance ground model is reasonably fast, but neglects atmospheric effects.

6.6 Mutual Coherence Function

The method for determining coherence between signals at the sensors in a receiving array is rather crude in comparison to the methods for determining mean levels described in the previous sections. The main reason for this shortcoming is a lack of knowledge of atmospheric propagation effects on second-order moments of acoustic fields. Second moments simply have not received as much research attention as the first moments (means).

The coherence equation used by ABFA, which is valid for line-of-sight propagation through inertial-subrange turbulence, is (Wilson, 1998b)

$$\Gamma(\rho) = \exp\left[-\frac{\pi k^2 R}{4}\left(0.464\frac{\hat{C}_T^2}{T_0^2} + 3.40\frac{\hat{C}_V^2}{c_0^2}\right)\rho^{5/3}\right]. \tag{24}$$

Here k is the wavenumber, R the total propagation distance, T_0 the ambient temperature in kelvins, c_0 the ambient sound speed, $\hat{C}_T^2$ the average structure-function parameter for temperature, $\hat{C}_V^2$ the average structure-function parameter for velocity, and ρ the separation between the sensors. The average structure-function parameters are found by integration over the propagation path:

$$\begin{aligned}\hat{C}_T^2 &= \frac{1}{R}\int_0^R C_T^2\left[z(\xi)\right]d\xi,\\ \hat{C}_V^2 &= \frac{1}{R}\int_0^R C_V^2\left[z(\xi)\right]d\xi.\end{aligned}$$

Height-dependent expressions for $C_T^2(z)$ and $C_V^2(z)$ are given in section 4.2.

7. Sensor Performance Predictions

7.1 Signal-to-Noise Ratio

The SNR provides a very good indication of sensor performance. Generally, if the SNR is well above 0 dB, the sensor will function satisfactorily. On the other hand, negative SNR normally indicates that the sensor will yield little useful information. The SNR (in decibels) simply equals the received signal level (RL) less the noise level (NL):

$$\mathrm{SNR} = \mathrm{RL} - \mathrm{NL}.$$

The received signal level is simply the sum of the source level (SL) (as would be measured at 1 m in free space) and the transmission loss as determined by the propagation model:

$$\mathrm{RL} = \mathrm{SL} + \mathrm{TL}. \tag{25}$$

The most important noise source in most low-frequency detection scenarios is wind noise. ABFA models the spectrum of the wind noise (WL) using the following empirical equation:

$$\mathrm{WL} = \max\left[40\left(1 - \frac{\log f - \log 20}{\log 500 - \log 20}\right) + 2.7U,\ 0\right], \tag{26}$$

where U is the wind speed in meters per second (calculated with the atmospheric model). The units of WL are given in decibels re 10^{-12} W per one-third octave band. Equation (26) was determined by curve-fitting to the data plotted in figure 5.60 of Beranek (1988). These data were recorded by a microphone with a 9-cm-diameter windscreen. The following equation relates WL in decibels to the corresponding spectrum $S_W(f)$ in power units:

$$\mathrm{WL} = 10\log S_W(f).$$

Besides the wind noise, ABFA also incorporates an environmental noise background, $S_E(f)$. Various values are assigned to $S_E(f)$ depending on the user's selection from such choices as "rural or forest" and "light battle."

To find the total noise level, ABFA integrates $S_E(f)$ and $S_W(f)$ over the bandwidth of the source:

$$\mathrm{NL} = 10\log\int_{f_\ell}^{f_u}\left[S_E(f) + S_W(f)\right]df. \tag{27}$$

7.2 Probability of Detection: Single Receiver

In most situations, the SNR at a receiver undergoes significant fluctuations. These fluctuations can be attributed, in part, to random changes in the background noise level, or to changes in the source (target) power output. The SNR fluctuations also occur as a result of random propagation effects, such as scattering by atmospheric turbulence. Because of the random nature of the SNR, we cannot say with certainty whether a source will be detected in a given environment. Rather, only a *probability of detection* can be specified. Actually, there are four possible events in a detection scenario, each having its own associated probability:

1. No source (target) is present, but the detection algorithm incorrectly deduces that a source is present. This is called a *false alarm*, the probability of which is denoted as P_{fa}.
2. No source is present, and the detection algorithm correctly deduces that no source is present. The probability of this event is $1 - P_{fa}$.
3. A source is present, and the detection algorithm correctly deduces that the source is present. This is called a *detection*, with probability P_D.
4. A source is present, but the detection algorithm incorrectly deduces that no source is present. This is called a *false dismissal*, with probability $P_{fd} = 1 - P_D$.

Obviously, we would like to have as high a detection probability as possible, while undergoing few false alarms. These two desires must be balanced against one another. If we set the threshold of our detector to a very low value, there will be a lot of false alarms, but we have an excellent chance of detecting a real target when one comes along. A high threshold produces fewer false alarms, but may cause us to miss a target. A popular method for formulating this trade-off, and the method used by ABFA, is the *Neyman-Pearson criterion*. It is described in some detail by Burdic (1984) and many other authors; in this report only a summary is provided.

When a source is not present, the received signal power $a_0(t)$ consists entirely of noise $n(t)$:

$$a_0(t) = n(t). \tag{28}$$

When the source is present, the received power $a_0(t)$ contains the source signal $s(t)$ as well as noise:

$$a_1(t) = s(t) + n(t). \tag{29}$$

The received signal power in each of these cases has a distinct probability density function (pdf). We indicate the pdf's for the two cases as $p_0(a)$ and $p_1(a)$, respectively.

Suppose we select a threshold γ, below which it is assumed that no source is present, and above which it is assumed that a source is present. The probability of a false alarm is then

$$P_{fa} = \int_{\gamma}^{\infty} p_0(a)\ da. \tag{30}$$

The probability of detection is

$$P_D = \int_{\gamma}^{\infty} p_1(a)\ da, \tag{31}$$

and the probability of false dismissal is

$$P_{fd} = \int_{0}^{\gamma} p_1(a)\ da = 1 - P_D. \tag{32}$$

The Neyman-Pearson criterion consists of fixing P_{fa} to some desired value, and then determining the threshold γ corresponding to this value of P_{fa}, using equation (30). This procedure obviously requires a model for $p_0(a)$. Once the value for γ has been obtained, we can compute P_D from a model for $p_1(a)$ using equation (31).

In general it is quite a difficult problem to determine the pdf's for signals propagated through the atmosphere. Let us assume initially that the signals are *fully saturated*. This means that atmospheric turbulence has broken up the deterministic signal into a large number of statistically independent contributions having random phases. The statistics for such strongly scattered signals are well known. Specifically, if the signal is regarded as complex (as is conventional in acoustics and many other fields involving wave propagation), the real and imaginary parts are zero-mean, Gaussian random variables (rv's) having the same variance $\sigma^2/2$ (Tatarskii, 1971). The complex signal corresponding to $s(t)$, for example, is written

$$\mathbf{s}(t) = \sqrt{s(t)} \exp\left[i\left(\omega t + \phi(t)\right)\right] = s_R(t) + i s_I(t), \tag{33}$$

where s is the signal magnitude squared, ϕ is the phase, $\omega = 2\pi f$ is the angular frequency, s_R is the real part, and s_I is the imaginary part. Note that s equals the sum of the squares of two independent Gaussian rv's:

$$s(t) = \mathbf{s}(t)\,\mathbf{s}^*(t) = s_R^2(t) + s_I^2(t).$$

(The asterisk indicates the complex conjugate.) It can be shown that s in this case has an *exponential* pdf:

$$p(s) = \frac{1}{\sigma^2} \exp\left(-\frac{s}{\sigma^2}\right) H(s), \tag{34}$$

where $H(x)$ is the Heaviside function (0 for $x < 0$ and 1 otherwise), and σ^2 is the variance of s. It can be shown that $\langle s \rangle = \sigma^2$. ABFA uses this relationship to determine σ^2.

For the pdf of the noise, ABFA uses a *chi-squared* distribution. A chi-squared pdf of order ν corresponds to the sum of ν independent, zero-mean Gaussian random variables, each having the same variance σ_n^2. It is given by

$$p_0(a) = \frac{\left(a/\sigma_n^2\right)^{\nu/2-1}}{\sigma_n^2 2^{\nu/2} \Gamma(\nu/2)} \exp\left(-\frac{a}{2\sigma_n^2}\right) H(a). \tag{35}$$

It can be shown that the mean value of a for the chi-squared distribution is $\langle a \rangle = \nu\sigma_n^2$. Hence if the mean signal level and ν are specified, the variance becomes fixed. The chi-squared pdf is plotted for several values of ν in figure 7, with $\langle a \rangle = 1$. Note that as ν is increased, the pdf becomes a delta function centered on the mean. The limit $\nu \to \infty$ therefore corresponds to a constant noise background.

Note that when $\nu = 2$, the chi-squared pdf reduces to an exponential pdf. Physically, one might think of $\nu/2$ roughly as the number of independent,

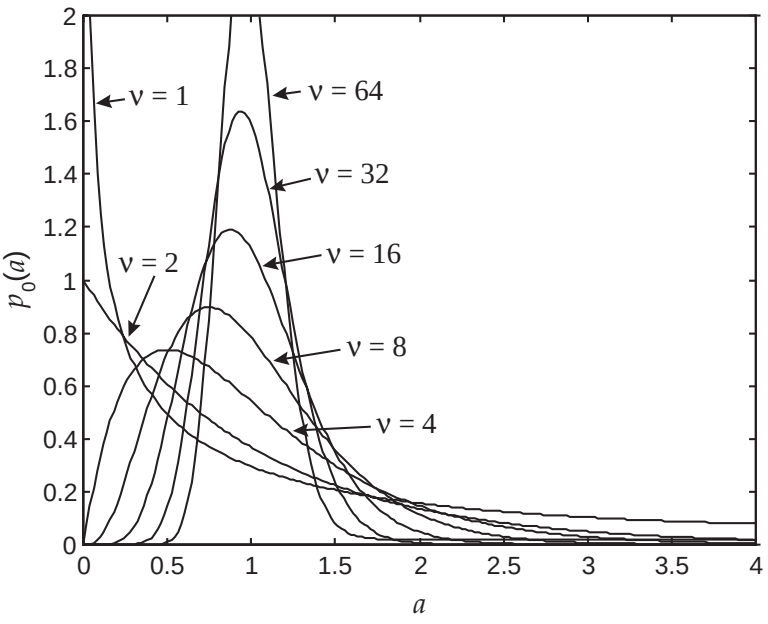

Figure 7. Probability density function for a chi-squared random variable. Mean is set to one, and parameter is number of degrees of freedom.

complex signals contributing to the total noise. If there are very few noise sources (small ν), the mean intensity can undergo dramatic fluctuations. If there are many noise sources (large ν), the noise background is nearly constant. (Think of the sound created by a few crickets chirping, as opposed to a field full of crickets.) It should be stressed, though, that one should not be too literal in interpreting $\nu/2$ as the number of independent noise sources. The assumptions inherent to the chi-squared pdf (strong scattering, independent noise sources of equal variance) are unlikely to be satisfied in a given situation. Therefore it is more reasonable to view equation (35) as a qualitative model whose parameters need to be determined empirically.

Let us now determine the probability of false alarm using the chi-squared pdf. The integral we need to solve is

$$P_{fa} = \int_{\gamma}^{\infty} \frac{\left(a/\sigma_n^2\right)^{\nu/2-1}}{\sigma_n^2 2^{\nu/2}\Gamma\left(\nu/2\right)} \exp\left(-\frac{a}{2\sigma_n^2}\right)\, da.$$

By defining $a' = a/2\sigma_n^2$, we have

$$P_{fa} = \frac{1}{\Gamma\left(\nu/2\right)} \int_{\gamma/2\sigma_n^2}^{\infty} \left(a'\right)^{\nu/2-1} \exp\left(-a'\right)\, da'.$$

The integral can now be expressed easily in terms of the incomplete gamma function, defined as (Abramowitz and Stegun, 1965, eq (6.5.1))

$$P\left(a, x\right) = \frac{1}{\Gamma\left(a\right)} \int_0^x e^{-t} t^{a-1}\, dt, \tag{36}$$

where $\Gamma\left(\right)$ is the ordinary (complete) gamma function. The result is

$$P_{fa} = 1 - P\left(\frac{\nu}{2}, \frac{\gamma}{2\sigma_n^2}\right). \tag{37}$$

There is no way to solve this equation for γ in closed form. However, it is fairly easy to solve using numerical methods such as the bisection technique.

Next let us determine the probability of detection. Since the signal in this case is the sum of two rv's, the pdf $p_1\left(a\right)$ is found by convolution of the pdf's of the two rv's (Bendat and Piersol, 1986):

$$p_1\left(a\right) = \int_{-\infty}^{\infty} p_0\left(z\right) p\left(a - z\right)\, dz.$$

Substituting this integral into equation (31) and changing the order of integration, we find

$$P_D = \int_{-\infty}^{\infty} p_0\left(z\right) \left[\int_{\gamma}^{\infty} p\left(a - z\right)\, da\right] dz.$$

Using equation (34), we evaluate the inner integral as

$$\int_{\gamma}^{\infty} p\left(a-z\right)\, da = \begin{cases} \exp\left[-\left(\gamma-z\right)/\sigma^2\right], & z<\gamma, \\ 1, & z \geq \gamma. \end{cases}$$

When this result is substituted back into the outer integral, we have

$$\begin{aligned} P_D &= \frac{1}{2\sigma_n^2 \Gamma\left(\nu/2\right)} \left[\exp\left(-\frac{\gamma}{\sigma^2}\right) \int_0^{\gamma} \left(\frac{z}{2\sigma_n^2}\right)^{\nu/2-1} \exp\left[-z\left(\frac{\sigma^2/2-\sigma_n^2}{\sigma^2\sigma_n^2}\right)\right] dz \right. \\ &\quad \left. + \int_{\gamma}^{\infty} \left(\frac{z}{2\sigma_n^2}\right)^{\nu/2-1} \exp\left(-\frac{z}{2\sigma_n^2}\right)\, dz \right]. \end{aligned}$$

Setting $z'' = z/2\sigma_c^2$ in the first integral, where

$$\sigma_c^2 = \frac{\sigma^2\sigma_n^2}{\sigma^2 - 2\sigma_n^2}, \tag{38}$$

and $z' = z/2\sigma_n^2$ in the second integral, we have

$$\begin{aligned} P_D &= \frac{1}{\Gamma\left(\nu/2\right)} \left[\exp\left(-\frac{\gamma}{\sigma^2}\right) \left(\frac{\sigma_c^2}{\sigma_n^2}\right)^{\nu/2} \int_0^{\gamma/2\sigma_c^2} \left(z''\right)^{\nu/2-1} \exp\left(-z''\right)\, dz'' \right. \\ &\quad \left. + \int_{\gamma/2\sigma_n^2}^{\infty} \left(z'\right)^{\nu/2-1} \exp\left(-z'\right)\, dz' \right]. \end{aligned}$$

The integrals are easily evaluated in terms of the incomplete gamma function (eq (36)), with result

$$\begin{aligned} P_D &= 1 - P\left(\frac{\nu}{2}, \frac{\gamma}{2\sigma_n^2}\right) + \exp\left(-\frac{\gamma}{\sigma^2}\right) \left(\frac{\sigma_c^2}{\sigma_n^2}\right)^{\nu/2} P\left(\frac{\nu}{2}, \frac{\gamma}{2\sigma_c^2}\right) \\ &= P_{fa} + \exp\left(-\frac{\gamma}{\sigma^2}\right) \left(\frac{\sigma_c^2}{\sigma_n^2}\right)^{\nu/2} P\left(\frac{\nu}{2}, \frac{\gamma}{2\sigma_c^2}\right). \end{aligned} \tag{39}$$

Note that the probability of detection is always greater than the probability of false alarm. This is because the power in the signal is always higher, on average, when the source is present.

Some example curves for P_D, as a function of P_{fa}, are shown in figure 8. I created these curves by determining the threshold γ from P_{fa}, using equation (37). The mean signal level $\langle s \rangle$ was set to 1. The mean noise level $\langle n \rangle$ then follows from the SNR in decibels according to

$$\mathrm{SNR} = 10 \log \frac{\langle s \rangle}{\langle n \rangle}. \tag{40}$$

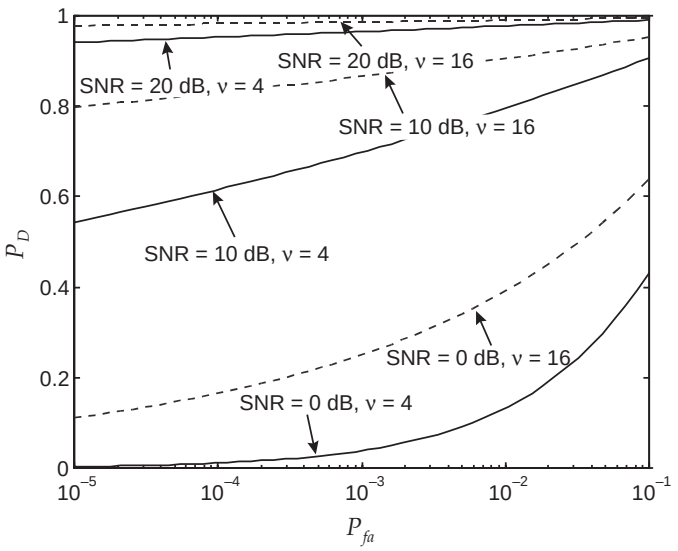

Figure 8. Probability of detection P_D as a function of probability for false alarm P_{fa} for a single sample of received signal. An exponential pdf was used for source level fluctuations, whereas a chi-squared pdf was used for backgrond noise. Signal-to-noise ratio (SNR) and degrees of freedom in chi-squared pdf are parameters.

Last, the variances follow from the relations $\sigma^2 = \langle s \rangle$, and $\sigma_n^2 = \langle n \rangle / \nu$.

The curves in figure 8 show that P_D increases with increasing P_{fa}, as one would expect. It is also clear that detection is much better when the SNR is high. Increasing ν favors detection somewhat, particularly at low SNR. It should be pointed out that the highest values of P_{fa} on the plot, 0.1, would be much too high in most practical situations. For example, if an effort is made every 1 min to detect a source, false alarms would occur every 10 min on the average. It would be impractical to investigate possible detections so frequently. Hence false alarm rates of, say, 10^{-3} or less are much more realistic.

7.3 Probability of Detection: Multiple Receivers

The analysis in the previous section assumed that just one receiver (sensor) is used to detect the source. But what happens if data from multiple receivers are merged?

It is actually easiest to address the multiple-receiver problem in terms of probabilities of false dismissals. Suppose there are N receivers. Let us indicate the probability of false dismissal for one of the receivers i as $P_{fd,i} = 1 - P_{D,i}$. Since the probability of occurrence for multiple events is found by multiplication of the probabilities for the individual events, the probability of false dismissal by *all* the receivers is

$$P_{fd} = \prod_{i=1}^{N} P_{fd,i}. \tag{41}$$

Hence the probability of detection by *one* of the receivers is

$$P_D = 1 - P_{fd} = 1 - \prod_{i=1}^{N} (1 - P_{D,i}) \,. \tag{42}$$

In addition to the possibility of multiple receivers, we need to account for the fact that a single receiver may be used to collect multiple samples. This problem is quite similar to the multiple-receiver problem. Suppose that a total of M_i statistically independent samples are collected and analyzed by receiver i. If the source of interest is not present, the probability of *not* having a false alarm in a single sample is $(1 - P_{fa,i})$, and the probability of having no false alarms at all is $(1 - P_{fa,i})^{M_i}$. Hence the probability that there will be *any* false alarms among the M_i samples is

$$\bar{P}_{fa,i} = 1 - (1 - P_{fa,i})^{M_i} \,. \tag{43}$$

Similarly, if M_i samples are collected while the source is present, the probability that the source will be detected among *any* of the samples is

$$\bar{P}_{D,i} = 1 - (1 - P_{D,i})^{M_i} \,. \tag{44}$$

In a given scenario, it would normally be the trade-off between $\bar{P}_{fa,i}$ and $\bar{P}_{D,i}$ that is of interest, as opposed to the trade-off between $P_{fa,i}$ and $P_{D,i}$. (Note that the two are the same, however, when $M_i = 1$.) Hence it is appropriate to use $\bar{P}_{D,i}$, rather than $P_{D,i}$, in equation (42). We can determine the relationship between $\bar{P}_{fa,i}$ and $\bar{P}_{D,i}$ for a specified M_i by first solving (43) for $P_{fa,i}$:

$$P_{fa,i} = 1 - (1 - \bar{P}_{fa,i})^{1/M_i} \,. \tag{45}$$

This value for $P_{fa,i}$ can then be used in the single-receiver analysis described in the previous section. The resulting value for $P_{D,i}$ is then simply substituted into equation (44). Figure 9 shows the results of such a calculation, for several values of M_i (1, 2, 4, and 10). Clearly, detection is enhanced when multiple independent samples can be collected.

The number of independent samples M_i is related to the time duration $\mathcal{T}_i$ of the data records processed by the sensing algorithm. The quantity $\mathcal{T}_i$ is called the *sensor integration time* by AFBA. ABFA estimates M_i by dividing $\mathcal{T}_i$ by the turbulence time scale. For propagation near the ground, the appropriate turbulence time scale is z/u_*.* Hence

$$M_i \simeq \max\left(1, \frac{\mathcal{T}_i u_*}{z}\right) . \tag{46}$$

*The equation for the turbulence time scale is a very rough estimate, and is valid only when wind-shear-generated turbulence dominates the scattering. This equation results from dimensional analysis, with z being the relevant length scale in a shear layer, and u_* (the friction velocity) being the relevant velocity scale.

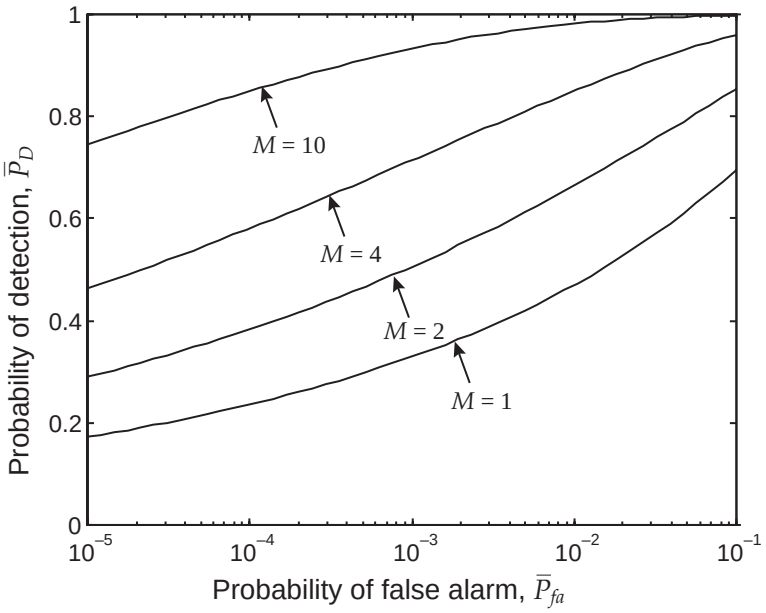

Figure 9. Probability of detection $\bar{P}_D$ as a function of probability for a false alarm $\bar{P}_{fa}$ for multiple samples of received signal. SNR is 0 dB, and degrees of freedom in background noise is $\nu = 16$. M is number of statistically independent samples.

The reason for placing a lower bound of 1 on the value of M_i is that any sample by the sensor produces at least one statistically independent data point. When the sensor listens for intervals longer than the turbulence time scale, more independent samples are produced.

7.4 Probability of Detection: Unsaturated Signals

In section 7.2 it was assumed that the signal to be detected was fully saturated. This assumption allowed us to derive an equation for the probability of detection in closed form. More generally, signals may have varying degrees of saturation. The pdf for an unsaturated signal has a *Rice-Nakagami* probability density function (Flatté *et al*, 1979):

$$p(s) = \frac{1}{\sigma^2} \exp\left(-\frac{s+m^2}{\sigma^2}\right) I_0\left(\frac{2\sqrt{s}m}{\sigma^2}\right) H(s), \tag{47}$$

where $I_0()$ is the modified Bessel function. In the limit $m \to 0$, equation (47) reduces to (34).

From equation (32) and the fact that the pdf of the sum of two rv's is given by the convolution of the pdf's, we find

$$\begin{aligned} P_D &= 1 - \int_0^\gamma p_1(a)\, da \\ &= 1 - \int_0^\gamma \left[\int_{-\infty}^{\infty} p_0(a-z)\, p(z)\, dz\right] da. \end{aligned}$$

Changing the order of integration, and using the property that both p_0 and p are zero when their arguments are less than zero, we obtain

$$P_D = 1 - \int_0^\gamma \left[\int_0^\gamma p_0 \left(a - z \right) \, da \right] p \left(z \right) \, dz.$$

If the pdf for the noise intensity is still assumed to be chi-square, as specified by equation (35), the inner integral can be expressed as an incomplete gamma function, and we have

$$P_D = 1 - \int_0^\gamma P \left(\frac{\nu}{2}, \frac{\gamma - z}{2\sigma_n^2} \right) p \left(z \right) \, dz. \tag{48}$$

This equation actually is valid for any $p\left(s\right)$. When equation (47) is specifically used for $p\left(s\right)$, the integration must be done numerically. This makes calculation of the detection probability for unsaturated signals more computationally intensive than for fully saturated signals.

The parameter m can be determined with equation (8.3.9) from Flatté *et al* (1979), after the equation is rescaled by the signal intensity:

$$m = \sqrt{\langle s \rangle} \exp \left(-\frac{1}{2} \Phi^2 \right). \tag{49}$$

In this equation, Φ is called the *strength parameter* of the turbulence. The strength parameter is given by

$$\Phi^2 = 2k_0^2 RL \left\langle \mu^2 \right\rangle, \tag{50}$$

where k_0 is the acoustic wavenumber, R is the propagation distance, L is the integral length scale, and $\langle \mu^2 \rangle$ is the index-of-refraction variance. ABFA uses the atmospheric model (sect. 4) to estimate the strength parameter. Once m has been determined, the signal variance parameter σ^2 follows from the relationship $\langle s \rangle = \sigma^2 + m^2$, which can be proven with equation (47).

7.5 Target Direction-Finding Accuracy

Acoustic sensor arrays determine the direction of a source by estimating the angle at which the acoustic wavefronts arrive at the array. The method used by ABFA for determining the accuracy of acoustical bearing estimates is discussed in detail elsewhere (Wilson, 1997a). Here only a summary of the method is given.

It can be shown that the variance of the angle-of-arrival estimates $\hat{\psi}$ about the actual value ψ is always greater than or equal to the inverse of a quantity known as the Fisher information matrix $\mathbf{J}$:

$$\left\langle \left(\psi - \widehat{\psi} \right)^2 \right\rangle \geq \mathbf{J}^{-1}(\psi). \tag{51}$$

(In the case considered here, involving only a single source, $\mathbf{J}$ is a scalar.) The right-hand side of equation (51) is called the *Cramer-Rao lower bound* (CRLB). Song and Ritcey (1996) show, for signals having a joint-Gaussian probability distribution, that

$$\mathbf{J}(\psi) = M \operatorname{tr}\left(\mathbf{R}_{aa}^{-1} \frac{\partial \mathbf{R}_{aa}}{\partial \psi} \mathbf{R}_{aa}^{-1} \frac{\partial \mathbf{R}_{aa}}{\partial \psi} \right), \tag{52}$$

where M is the number of statistically independent samples (see sect. 7.2), and $\mathbf{R}_{aa}$ is the cross-correlation matrix for the signals received at each of the sensors, defined by

$$\mathbf{R}_{aa}(\psi) = \langle \mathbf{a}(\psi, t) \widetilde{\mathbf{a}}(\psi, t) \rangle, \tag{53}$$

in which $\mathbf{a}(\psi, t)$ is a column vector whose elements are the time-varying acoustic pressure signals at each of the N sensors in the array. As before, we can decompose $\mathbf{a}(\psi, t)$ into contributions from the source of interest and noise:

$$\mathbf{a}(\psi, t) = \mathbf{s}(\psi, t) + \mathbf{n}(t). \tag{54}$$

Assuming that the source signal and noise are uncorrelated, the received signal cross-correlation matrix becomes the sum of $\mathbf{R}_{ss}(\psi) = \langle \mathbf{s}(\psi, t) \widetilde{\mathbf{s}}(\psi, t) \rangle$ and $\mathbf{R}_{nn} = \langle \mathbf{n}(t) \widetilde{\mathbf{n}}(t) \rangle$:

$$\mathbf{R}_{aa}(\psi) = \mathbf{R}_{ss}(\psi) + \mathbf{R}_{nn}. \tag{55}$$

Assuming furthermore that the noise at the individual sensors is mutually uncorrelated and equal in variance, we have

$$\mathbf{R}_{aa}(\psi) = \mathbf{R}_{ss}(\psi) + \sigma_n^2 \mathbf{I}, \tag{56}$$

where σ_n^2 is the noise variance. When the signals and noise are normalized so that $\mathbf{s}(\psi, t)$ has unit variance, σ_n^2 becomes a noise-to-signal variance ratio. It is related to the SNR (in decibels) by

$$\mathrm{SNR} = -10 \log \sigma_n^2. \tag{57}$$

Following Wilson (1997a), the source signal correlation matrix is written in the form

$$\mathbf{R}_{ss}(\psi) = \mathbf{S}(\psi) \odot \mathbf{T},$$

where $\mathbf{S}(\psi)$ is called the *array steering matrix*, and $\mathbf{T}$ accounts for the imperfect coherence of the signal across the array due to turbulence. The symbol $\odot$ indicates the Hadamard matrix product (simple element-by-element multiplication). The steering matrix depends on the phase delays between the sensors; the element in the mth row and nth column is the phase delay between sensors m and n in the array. This delay is given by

$$S_{mn}(\psi) = \exp\left[-ikd_{mn}\cos\left(\psi - \alpha_{mn}\right)\right], \tag{58}$$

where

$$d_{mn}^2 = (x_n - x_m)^2 + (y_n - y_m)^2$$

is the sensor separation, and (x_n, y_n) is the location of sensor n;

$$\alpha_{mn} = \arctan\left[(y_n - y_m)/(x_n - x_m)\right]$$

is the angle between the sensors.

The elements of the matrix describing the turbulence effect are equal to the mutual coherence function (MCF), evaluated at the sensor separation:

$$T_{mn} = \Gamma(d_{mn}). \tag{59}$$

The MCF is discussed in section 6.6.

7.6 Target Location-Finding Accuracy

When the data from two or more direction-finding arrays are merged, it is possible to estimate the actual location of a source. ABFA calculates the uncertainty in such location estimates using a very general, inverse problem formulation (Aki and Richards, 1980; Wilson and Thomson, 1994).

Suppose that the angles-of-bearing estimates from N sensor arrays are used to estimate the location of the source. The locations of the N arrays, (x_n, y_n), $n = 1, 2, \ldots, N$, are assumed to be known exactly. The location of the source (target), (x, y), is assumed to be known to within some uncertainty σ in both the x- and y-directions. (In ABFA, the initial uncertainties in the source position are set to the overall size of the domain. Note that the notation in this section differs somewhat from that in the previous one.) The full geometry of the problem is illustrated in figure 10.

The angle-of-bearing estimate produced by each of the arrays is used to reduce the initial uncertainty. Let ψ_n be the actual bearing of the source relative to each receiving array:

$$\tan\psi_n = \frac{y - y_n}{x - x_n}. \tag{60}$$

Figure 10. Geometry of inverse problem for location-finding accuracy.

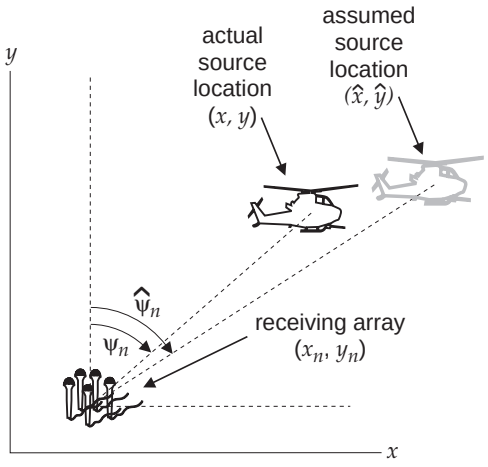

Now let us define $\hat{\psi}_n$ as the estimated (reference) direction of the source, and $(\hat{x}, \hat{y})$ its estimated location. The perturbations of the estimated position from the actual one are defined as

$$\psi'_n = \psi_n - \hat{\psi}_n, \quad x' = x - \hat{x}, \quad y' = y - \hat{y}.$$

In the context of inverse theory, the "knowns" (the ψ'_n) are usually called the *data*. Arranging the data as a column vector, we define

$$\mathbf{d} = \begin{bmatrix} \psi'_1 \\ \psi'_2 \\ \vdots \\ \psi'_N \end{bmatrix}.$$

The unknown perturbations x' and y' to be determined are called the *models*:

$$\mathbf{m} = \begin{bmatrix} x' \\ y' \end{bmatrix}.$$

The so-called *forward problem* consists of determining the data from the models. Equation (60) gives the solution to the forward problem. The *inverse problem* consists of solving for the models in terms of the data. Although solution of the inverse problem is far from trivial, it can be made much more tractable if we first linearize the forward problem, by keeping only the initial terms in the multivariate Taylor series expansions for the data. That is,

$$\psi'_n \simeq \left.\frac{\partial \psi_n}{\partial x}\right|_{\widehat{x,y}} x' + \left.\frac{\partial \psi_n}{\partial y}\right|_{\widehat{x,y}} y'.$$

The forward problem can be written in matrix notation as

$$\mathbf{d} = \mathbf{G}\mathbf{m} + \mathbf{n},$$

where the vector $\mathbf{n}$ represents the noise (uncertainty) in the data, and

$$\mathbf{G} = \begin{bmatrix} \partial\psi_1/\partial x & \partial\psi_1/\partial y \\ \vdots & \vdots \\ \partial\psi_N/\partial x & \partial\psi_N/\partial y \end{bmatrix}. \tag{61}$$

From the forward problem formulation, equation (60), we find

$$\left.\frac{\partial\psi_n}{\partial x}\right|_{\widehat{x},\widehat{y}} = -\frac{\sin\hat{\psi}_n \cos\hat{\psi}_n}{\hat{x} - x_n}, \quad \text{and} \tag{62}$$

$$\left.\frac{\partial\psi_n}{\partial y}\right|_{\widehat{x},\widehat{y}} = \frac{\sin\hat{\psi}_n \cos\hat{\psi}_n}{\hat{y} - y_n}. \tag{63}$$

Let us now consider the somewhat more complicated problem where the source is moving at a velocity (v_x, v_y). The bearing to the source is then given by equation (60), but with x and y replaced by the location where the sound was emitted. This location is $(x - v_x t, y - v_y t)$, where t is the time of emission. Hence

$$\tan\psi_n = \frac{y - v_y t - y_n}{x - v_x t - x_n}. \tag{64}$$

We can determine the time of emission by equating $c_0 t$ to the propagation distance:

$$c_0 t = \sqrt{(x - v_x t - x_n)^2 + (y - v_y t - y_n)^2}.$$

Solving this equation for t, one finds

$$t = \frac{v_x(x - x_n) + v_y(y - y_n) + \sqrt{[v_x(x - x_n) + v_y(y - y_n)]^2 + \left(c_0^2 - v_x^2 - v_y^2\right)\left[(x - x_n)^2 + (y - y_n)^2\right]}}{c_0^2 - v_x^2 - v_y^2}. \tag{65}$$

The matrix $\mathbf{G}$ for the forward problem generalizes to

$$\mathbf{G} = \begin{bmatrix} \partial\psi_1/\partial x & \partial\psi_1/\partial y & \partial\psi_1/\partial v_x & \partial\psi_1/\partial v_y \\ \vdots & \vdots & \vdots & \vdots \\ \partial\psi_N/\partial x & \partial\psi_N/\partial y & \partial\psi_N/\partial v_x & \partial\psi_N/\partial v_y \end{bmatrix}, \tag{66}$$

where

$$\left.\frac{\partial \psi_n}{\partial x}\right|_{\widehat{x},\widehat{y},\widehat{v}_x,\widehat{v}_y} = -\frac{\left(\sin\hat{\psi}_n + \widehat{v}_y/c_0\right)\cos\hat{\psi}_n}{\hat{x} - x_n}, \tag{67}$$

$$\left.\frac{\partial \psi_n}{\partial y}\right|_{\widehat{x},\widehat{y},\widehat{v}_x,\widehat{v}_y} = \frac{\sin\hat{\psi}_n\left(\cos\hat{\psi}_n + \widehat{v}_x/c_0\right)}{\hat{y} - y_n}, \tag{68}$$

$$\left.\frac{\partial \psi_n}{\partial v_x}\right|_{\widehat{x},\widehat{y},\widehat{v}_x,\widehat{v}_y} = \frac{\sin\hat{\psi}_n}{c_0}, \quad \text{and} \tag{69}$$

$$\left.\frac{\partial \psi_n}{\partial v_y}\right|_{\widehat{x},\widehat{y},\widehat{v}_x,\widehat{v}_y} = -\frac{\cos\hat{\psi}_n}{c_0}. \tag{70}$$

In ABFA, the estimated velocity $(\widehat{v}_x, \widehat{v}_y)$ is set by the user.

If $\mathbf{G}$ were an invertible matrix and the noise were negligible, we could now solve the inverse problem. Unfortunately, $\mathbf{G}$ is generally not invertible; in fact, it is not necessarily even a square matrix. Furthermore, uncertainties in the data are often substantial. Fortunately, methods for solving inverse problems such as this have been studied for decades in such areas as seismology, ocean acoustic tomography, and medical tomography. One of the simplest and most satisfactory methods for approximating the inverse is called the *stochastic inverse*, which minimizes the expected mean square difference between the model estimates and their actual values. (See, for example, Aki and Richards (1980), or Wilson and Thomson (1994).) The stochastic inverse is given by

$$\hat{\mathbf{m}}_s = \mathbf{G}_s^{-1}\mathbf{d}, \tag{71}$$

where

$$\mathbf{G}_s^{-1} = \mathbf{R}_{md}\mathbf{R}_{dd}^{-1}, \tag{72}$$

and

$$\mathbf{R}_{mm} = \left\langle \mathbf{m}\tilde{\mathbf{m}} \right\rangle, \tag{73}$$

$$\mathbf{R}_{nn} = \left\langle \mathbf{n}\tilde{\mathbf{n}} \right\rangle, \tag{74}$$

$$\mathbf{R}_{md} = \left\langle \mathbf{m}\tilde{\mathbf{d}} \right\rangle = \mathbf{R}_{mm}\tilde{\mathbf{G}}, \tag{75}$$

$$\mathbf{R}_{dd} = \left\langle \mathbf{d}\tilde{\mathbf{d}} \right\rangle = \mathbf{G}\mathbf{R}_{mm}\tilde{\mathbf{G}} + \mathbf{R}_{nn}. \tag{76}$$

The four equations above define the *model covariance matrix*, the *noise covariance matrix*, the *model-data covariance matrix*, and the *data covariance matrix*.

With regard to our problem involving acoustic source localization, we may assume that the initial uncertainties in the x- and y-coordinates of the

source are independent and both equal to a prescribed value σ_s^2. The initial uncertainty in the velocities is σ_v^2. Hence

$$\mathbf{R}_{mm} = \begin{bmatrix} \sigma_s^2 & 0 & 0 & 0 \\ 0 & \sigma_s^2 & 0 & 0 \\ 0 & 0 & \sigma_v^2 & 0 \\ 0 & 0 & 0 & \sigma_v^2 \end{bmatrix}. \tag{77}$$

The "noise," or data uncertainty, in this case is given by the CRLBs of the angle-of-arrival estimates, equation (51):

$$\mathbf{R}_{nn} = \begin{bmatrix} \mathbf{J}^{-1}(\psi_1) & 0 & \cdots & & \\ 0 & \mathbf{J}^{-1}(\psi_2) & & & \\ \vdots & & \ddots & 0 & \\ & & 0 & \mathbf{J}^{-1}(\psi_N) & \end{bmatrix}. \tag{78}$$

Our interest in an application such as ABFA is not in the estimated source positions themselves, but rather in the statistical uncertainties of the estimates. The uncertainty is given by the error covariance matrix

$$\mathbf{R}_{ee} = \langle \mathbf{e}\tilde{\mathbf{e}} \rangle, \tag{79}$$

where $\mathbf{e} = \mathbf{m} - \hat{\mathbf{m}}$. It can be shown (Wilson and Thomson, 1994) that

$$\mathbf{R}_{ee} = (\mathbf{W} - \mathbf{I})\,\mathbf{R}_{mm}\left(\widetilde{\mathbf{W}} - \mathbf{I}\right) + \mathbf{G}_s^{-1}\mathbf{R}_{nn}\widetilde{\mathbf{G}_s^{-1}}, \tag{80}$$

where $\mathbf{W} = \mathbf{G}_s^{-1}\mathbf{G}$ is called the *resolution matrix*. In our case, $\mathbf{R}_{ee}$ is a 4×4 matrix. The upper left element of $\mathbf{R}_{ee}$ is the expected variance of the x estimates about their actual values, whereas the lower right element corresponds to the variance in y.

To summarize, we have the following procedure for calculating the uncertainties in the source location estimates:

1. A source position is hypothesized. The uncertainty of the source actually residing at this position is set to the size of the simulated domain. Based on this information, the model covariance matrix, equation (77), is determined.
2. Equations (68) and (69) are used to determine the linearized forward problem solution $\mathbf{G}$, equation (61).
3. The propagation and noise models are run to calculate the SNR at each array position, for a source at the hypothetical position.

4. The SNR is used to calculate the CRLBs for the direction-finding performance of each array. The noise covariance matrix, equation (78), follows from the CRLBs.
5. Now that $\mathbf{R}_{mm}$, $\mathbf{R}_{nn}$, and $\mathbf{G}$ are known, $\mathbf{R}_{md}$ and $\mathbf{R}_{dd}$ follow immediately from equations (75) and (76), respectively. The stochastic inverse is then determined from equation (72).
6. The reduced uncertainty in the source position (the reduction being due to the information provided by the arrays) is given by equation (80).

8. Example Calculations

8.1 Transmission Loss

As discussed in section 6, the transmission loss (TL) indicates the energy lost by the sound wave as it propagates from the source to the receiver. The TL depends strongly upon environmental influences such as atmospheric winds and temperature, the absorptive properties of the ground, and the topography. Some example calculations are provided in this section to demonstrate these environmental influences.

Figure 11 shows a TL calculation for a 20-Hz source. This frequency is close to the fundamental frequency produced by many helicopters. The height of the source is 10 m above ground level. The height of the sensor is 0.1 m, and its horizontal position is varied across the simulation domain. The calculations were made based on the impedance ground model (sect. 6.2), with the ground type being long grass. Since the impedance ground model neglects atmospheric and topographic effects on the sound levels, the sound levels decay smoothly and omnidirectionally away from the source.

The TL calculation shown in figure 12 is essentially a repeat of figure 11, except that the hybrid wedge/impedance ground propagation model

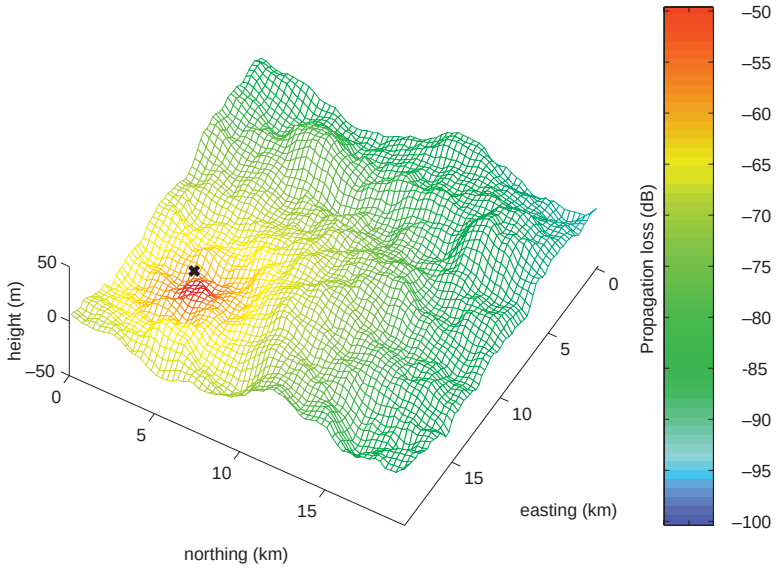

Figure 11. Transmission loss calculation for a 20-Hz source at 10-m height (hovering helicopter) over grass, using plain impedance ground model. Location of helicopter is marked by ×.

(sect. 6.5) was used. As a result, topographic effects (but not atmospheric effects) are incorporated into this calculation. The topography was synthesized with the von Kármán model, equation (7), for $L = 2500$ m, $\sigma = 20$ m, and $\nu = 1$. Enhancement of the sound levels is evident on the sides of the hills facing the source, whereas acoustic "shadows" form on hillsides shielded from the source.

Figure 13, like figure 12, uses the hybrid wedge/impedance ground model. However, the surface was changed from long grass to ice. Hard materials such as ice and rock absorb very little sound energy. As a result, the TL at long distances from the source is much reduced.

Figure 12. Same as figure 11, except that hybrid wedge/ground impedance model was used. Hence topographic effects on sound field are included.

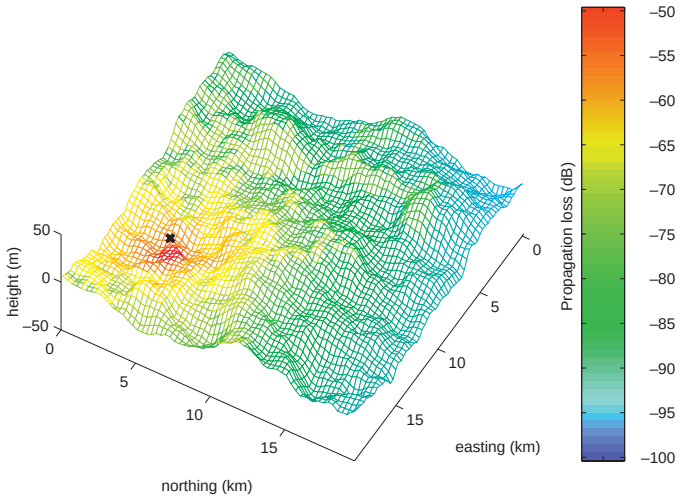

Figure 13. Same as figure 12, except that ground type was changed from grass to ice.

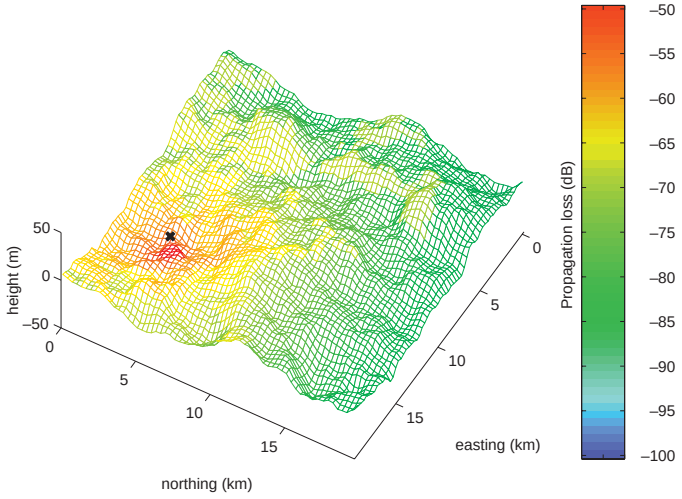

The next set of TL calculations, figures 14 to 16, are again for a 20-Hz source (helicopter) at 10 m over grassy ground, except that atmospheric refraction effects are incorporated into the calculations via the hybrid wedge/FFP model (sect. 6.5). The figures show calculations for three idealized meteorological conditions: mostly sunny and calm (table 1), overcast and windy (table 1), and a deep inversion characteristic of the late night or early morning under clear skies (Noble, 1994). For the mostly sunny and calm conditions (fig. 14), there is a sharp increase in temperature near the surface. As a result, sound energy is refracted upward, resulting in a large TL at distances greater than several kilometers.

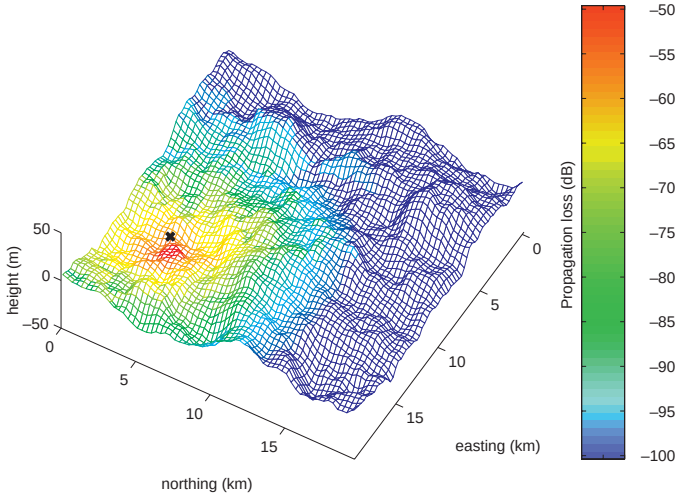

Figure 14. Same as figure 12, except that hybrid wedge/FFP propagation model was used. Hence both atmospheric and topographic effects on sound field are included. Atmospheric conditions are characteristic of a sunny, calm day.

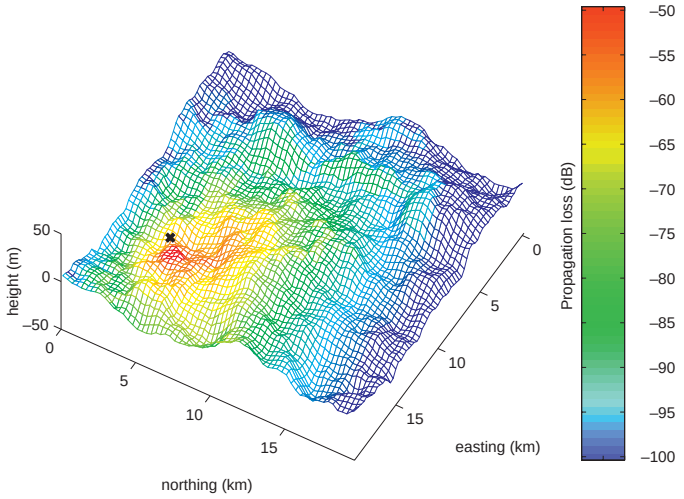

Figure 15. Same as figure 14, except that overcast, windy atmospheric conditions are used. Wind is blowing to north (from left to right, and slightly down, in figure).

Figure 16. Same as figure 14, except that deep inversion atmospheric conditions are used.

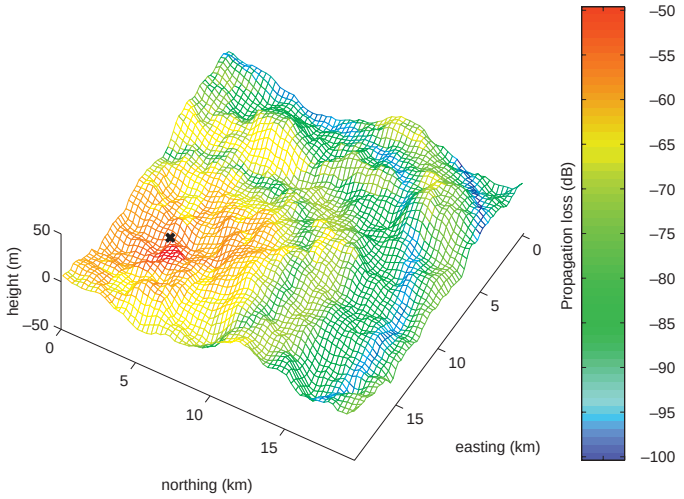

The overcast, windy case (fig. 15) features a strong wind blowing from the north. The wind speed is about 6.2 m/s at a height of 10 m. Because of this strong wind, the TL is much less downwind from the source than upwind. The deep inversion case (fig. 16) has a temperature gradient of +15 °C/km below 300 m, and −8 °C/km above. No wind is included in this case. The positive temperature gradient below 300 m results in pronounced trapping of sound energy near the ground. As a result, low TL is observed far from the source. "Skip zones," or isolated ranges of diminished sound levels, are also evident. The skip zones result from combined refraction/ground-reflection effects.

8.2 Signal-to-Noise Ratio

SNR calculations (sect. 7.1) incorporate the source level, TL, and environmental noise. Figures 17 to 19 show SNR calculations for the same three atmospheric conditions used in figures 14 to 16. The source level at 1 m in each case is 170 dB, which is characteristic of a loud source such as a helicopter. The bandwidth of the source is 1 Hz. The background noise is set to 30 dB per 1/3 octave band, which is a level characteristic of a quiet, natural setting. As a result, most of the noise is caused by turbulent pressure fluctuations on the microphone, or "wind noise."

Both the sunny, calm case and the overcast, windy case (fig. 17, 18) have SNRs favorable to detection (above 0 dB) within a radius 5 to 10 km from the source. The region of favorable SNR for these cases is small not only because of the high TL, but also because both cases feature strong turbulence and hence high levels of wind noise.

Figure 17. SNR calculation for a 20-Hz, 1-Hz-bandwidth source at 10-m height (hovering helicopter) over grass, using hybrid wedge/FFP model. Atmospheric profiles are characteristic of sunny, calm conditions. Noise background is characteristic of a quiet, natural setting. Location of helicopter is marked by ×.

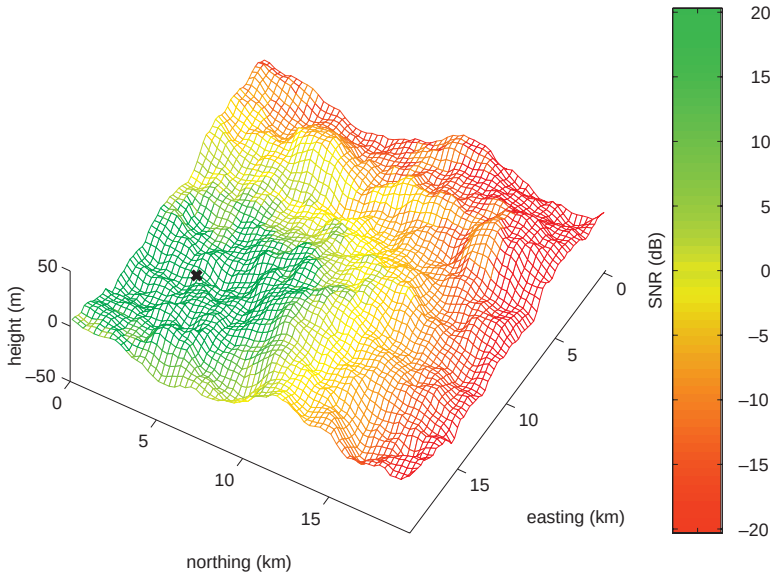

Figure 18. Same as figure 17, except that overcast, windy atmospheric conditions are used.

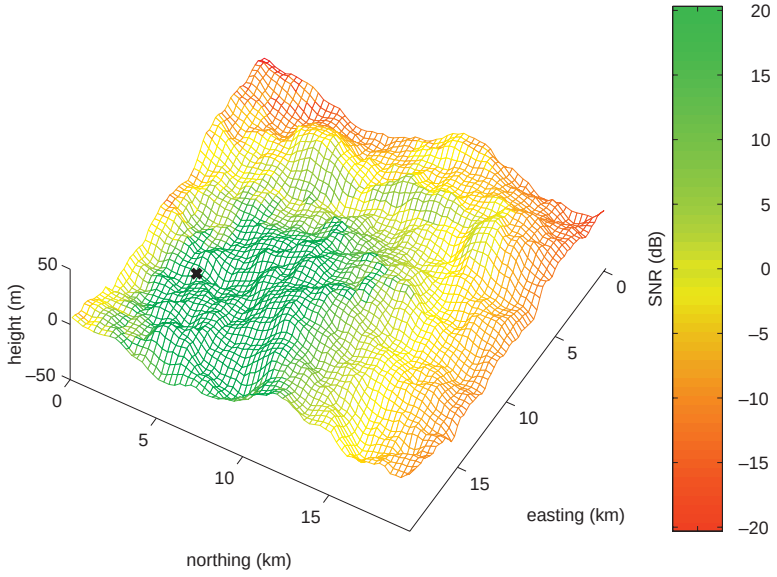

The deep inversion case (fig. 19) has no turbulence, and as a result the SNR is favorable for distances very far from the source. (In actuality, temperature inversion conditions often have low-intensity or intermittent episodes of turbulence. Because turbulence in such statically stable conditions is poorly understood at present, ABFA makes the simplification of setting the turbulence intensity to zero. The user can change the turbulence intensity to a nonzero value if desired.)

Figure 19. Same as figure 17, except that deep inversion atmospheric conditions are used.

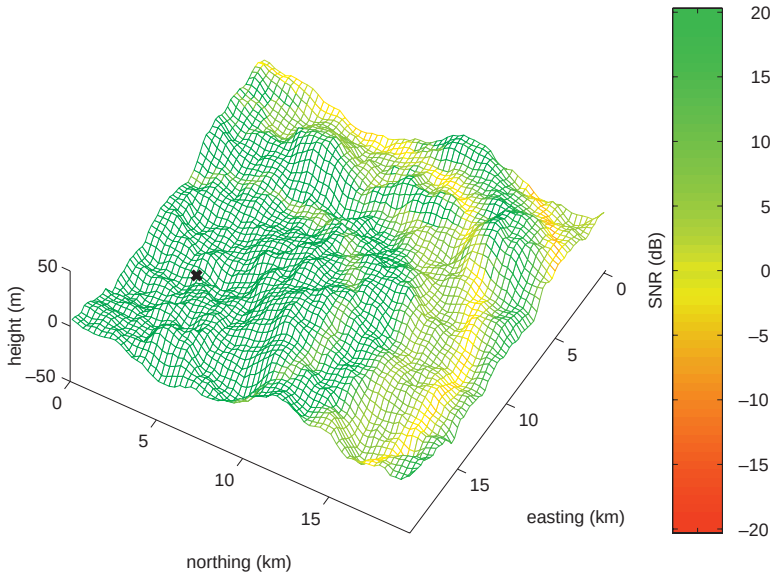

8.3 Probability of Detection

Probabilities of detection depend strongly upon the SNR. If the SNR is well above 0 dB, the source can generally be detected. But, as discussed in section 7.2, other factors related to the sensor and propagation environment also play a role in detection. Among these are the integration time of the sensor (how long it listens for the source signal), and the characteristic time of the signal fluctuations.

Figure 20 shows the probability of detection for the same helicopter-like source considered previously. Sunny, calm atmospheric conditions were used in the calculation. Unlike the previous figures, where the source position was fixed and the sensor position varied, in figure 20 the sensor position is fixed and the source position varies. The sensor is positioned at a height of 0.1 m above ground level, on an elevated region near the center of the simulation domain. Because of the elevated position of the sensor, terrain effects on detection are rather small. The sensor integration time used in the calculation was $\mathcal{T}$ = 10 s. The height of the propagation path was taken as 5.05, which is the average of the source and sensor heights. Since the friction velocity for the sunny, calm case is u_* = 0.1 m/s, the turbulence time scale is therefore 0.1/5.05 = 50.5, and the number of independent samples determined from equation (46) is $M = \max(1, 10/50.5) = 1$.

Figure 21 is similar to 20, except that the sensor integration time has been increased to $\mathcal{T}$ = 10 min. This larger value for $\mathcal{T}$ causes M to increase to 12, and the area of high probability of detection increases as a result. Figure 22

Figure 20. Probability of detecting a helicopter hovering over grass, for sunny, calm atmospheric conditions. Noise background is characteristic of a quiet, natural setting. Sensor integration time is 10 s. Sensor location (fixed) is marked by ○.

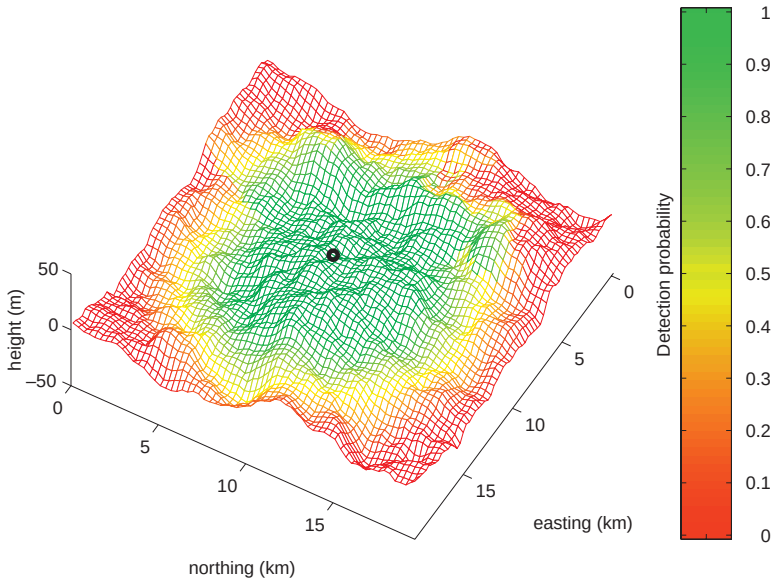

Figure 21. Same as figure 20, except that sensor integration time was increased 10 min.

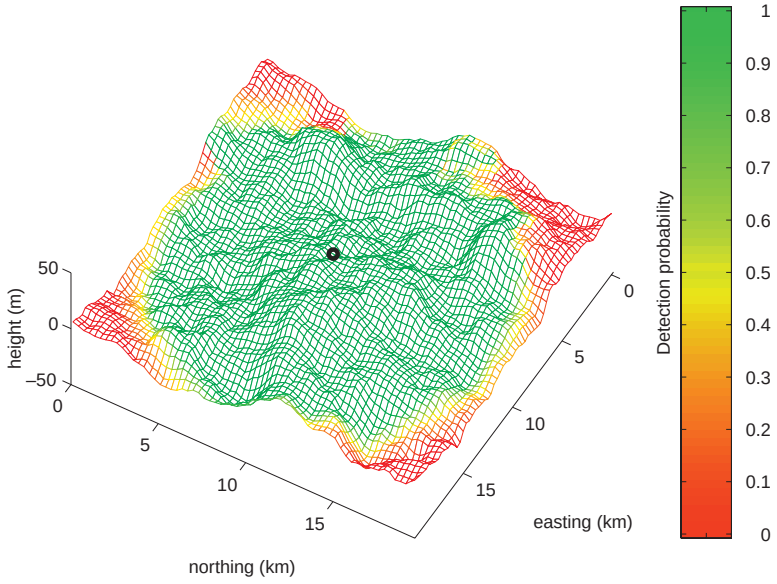

is also similar to 20, except that sensors at two locations, on opposite sides of a hill, have been included in the calculation. Together the two sensors provide good detection probability over most of the simulation domain, except in the northwest corner and a valley along the eastern edge. This figure demonstrates the utility of ABFA for determining good sensor locations.

Figure 22. Same as figure 20, except that two independent sensors are deployed.

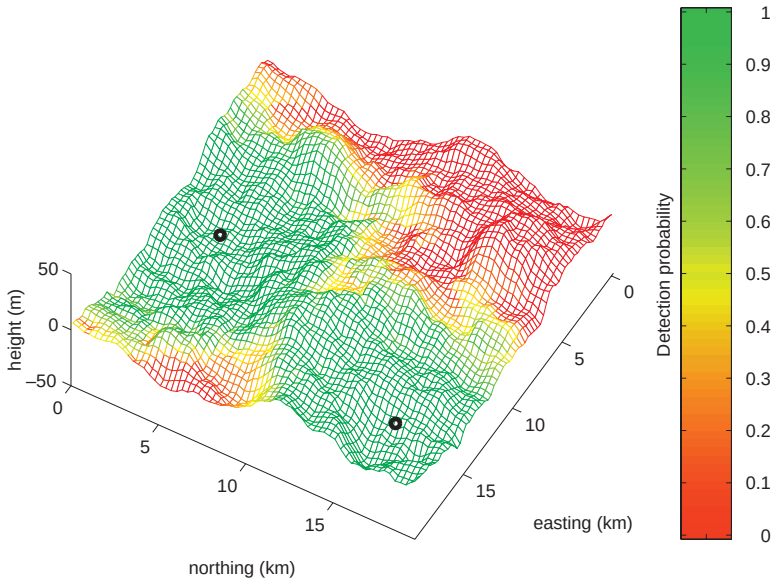

Figures 23 and 24 are similar to figure 20, except that different weather conditions were used. Specifically, overcast and windy conditions were used for figure 23, and the deep inversion profiles for figure 24. The sensor integration time for both figures was 10 s, which resulted in $M = 1$ in each instance. The region of high probability of detection has a dramatic asymmetry in figure 23 due to the strong wind effect. Conditions for detection are much improved when the source is upwind from the sensor. The probability of detection is high everywhere in the simulated domain for the deep inversion case (fig. 24), as a result of the high SNR.

8.4 Target Location-Finding Accuracy

As discussed in sections 7.5 and 7.6, an array of acoustic sensors can be used to determine the bearing of a target (source). Data from multiple arrays can then be combined to determine the target location. Some examples of the accuracy of target locations that can be obtained from multiple arrays are shown in figures 25 to 28. In each figure, six separate sensor arrays have been deployed within the simulation domain. Each array consists of six microphones, equally spaced along a circle of radius 1 m. Calculations are presented for the same three weather conditions used previously: sunny and calm (fig. 25 and 26), windy and overcast (fig. 27), and deep inversion (fig. 28). The target is the same as before: a 20-Hz source similar to a hovering helicopter.

Figure 23. Same as figure 20, except that overcast, windy atmospheric conditions are used.

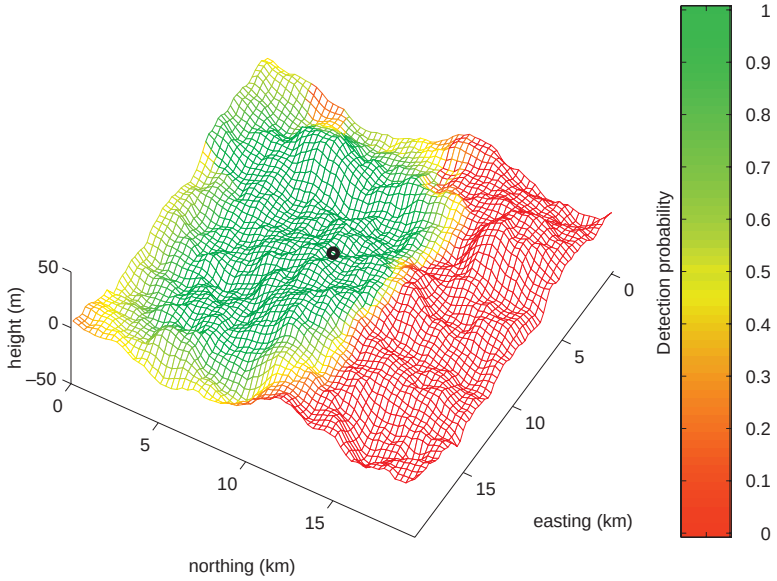

Figure 24. Same as figure 20, except that deep inversion atmospheric conditions are used.

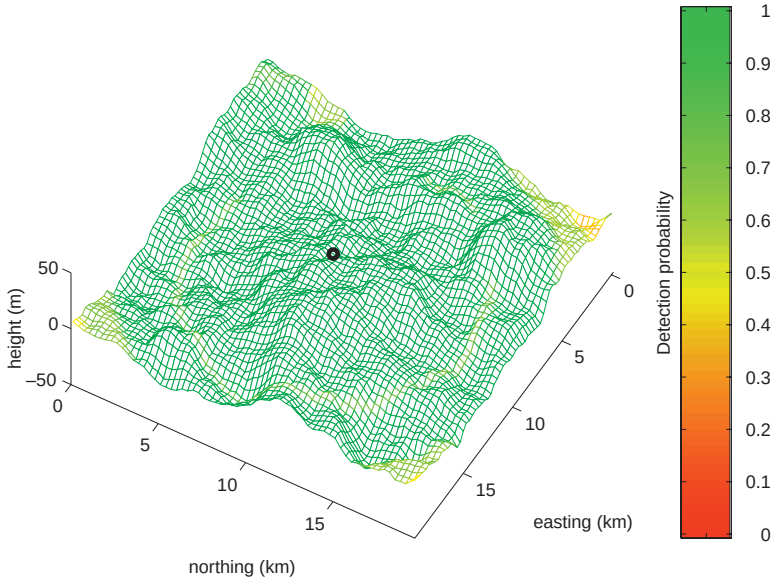

The target-location-finding accuracy is clearly best for the deep inversion conditions. According to the calculations, the location of the target can be determined to an accuracy better than a few hundred meters over much of the simulation domain. Although the location-finding accuracy for the cases with high turbulence (sunny and calm, and overcast and windy) is not as satisfactory, useful location information can still be obtained. The target location can be determined to better than 1 km in regions where the sensors are placed less than about 5 km apart. The main advantages of

Figure 25. Accuracy for resolving position of a target (hovering helicopter), under sunny, calm atmospheric conditions. Sensors, marked by ○'s, each consist of an array of six individual microphones. Sensors are positioned at high elevation points. Noise background is characteristic of a quiet, natural setting.

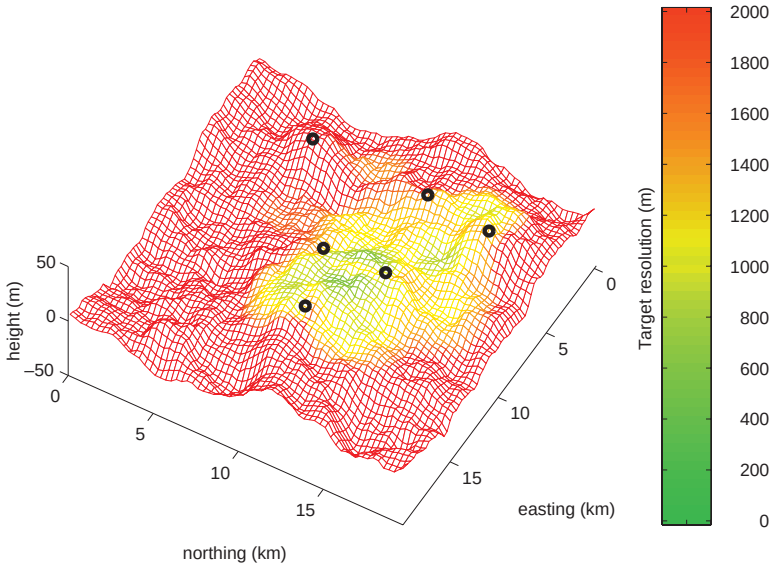

Figure 26. Same as figure 25, except that sensors are positioned along a semicircular valley.

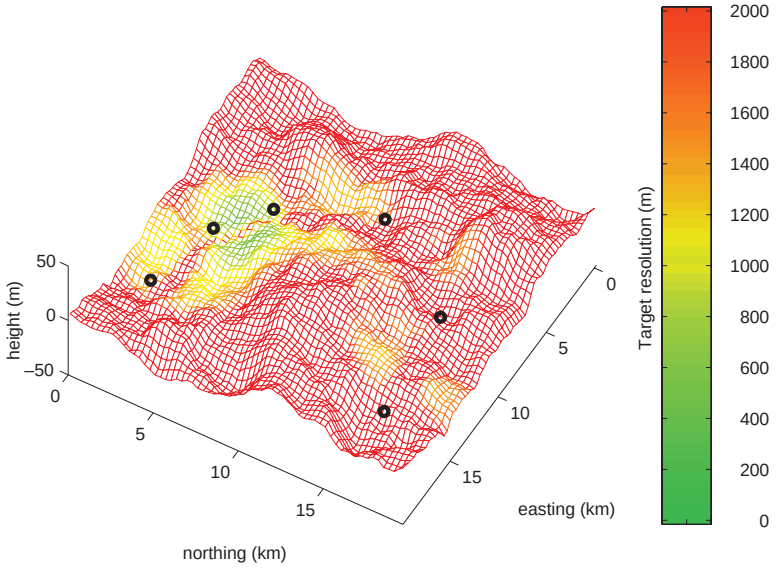

using acoustic sensors instead of radar in a scenario such as this would be low cost, insensitivity to ground clutter, and passive operation (i.e., the sensors themselves do not emit a detectable signal).

The two figures corresponding to sunny, calm conditions (25 and 26) contrast location-finding accuracy from two different sensor layouts. In figure 25, the arrays are closer to each other, and positioned on terrain features having high elevation. In figure 26, the arrays are placed in a low-elevation region having the appearence of a long, semicircular valley.

Figure 27. Same as figure 25, except that overcast, windy atmospheric conditions are used.

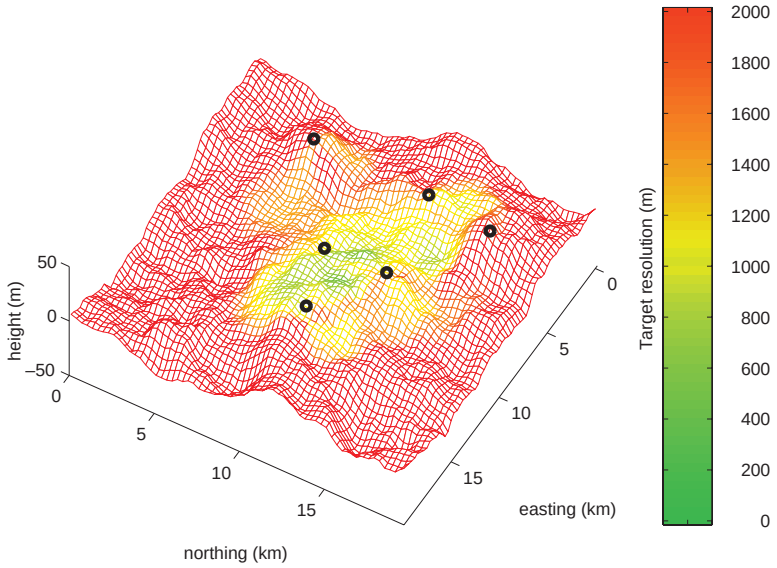

Figure 28. Same as figure 25, except that deep inversion atmospheric conditions are used.

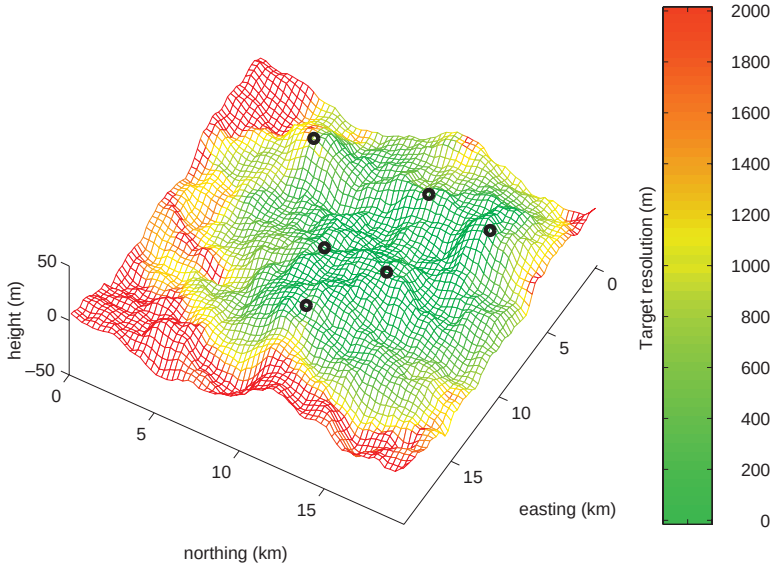

Although the spatial coverage of the different sensor configurations has a complicated appearance, it can be understood from a few basic observations. First, a single, isolated array is of no help in determining the *location* of a source; it can only determine *bearing*. Second, when an isolated pair of arrays occurs, the location of a target cannot be determined along the axis of the pair, since no triangulation is obtained from the directional information produced by each array. Therefore, only when three or more arrays are close enough to a target to yield accurate

directional information can the target location be accurately determined. For the layout in figure 26, there is no combination of three or more sensor arrays packed closely enough to yield a connected region of good coverage. On the other hand, the layout in figure 25 features five arrays that are close enough to provide a good, connected region of coverage. A sixth array (positioned at a northing of about 5 km, and easting 3 km) is too far removed from the other five to be useful in the location finding.

9. Concluding Remarks and Topics for Future Research

ABFA synthesizes many recent advances in computational acoustics, software capabilities, and information theory as applied to acoustic arrays. The result is a very flexible tool for evaluating the performance of acoustic sensor configurations in various environments. Although ABFA is a prototype, and perhaps not yet sufficiently refined for the general user, it incorporates many ideas that can serve as useful starting points for future development.

The prediction methods incorporated into ABFA are generally state of the art. Still, there remains much need for critical examination and evaluation of some of the underlying equations and techniques used for propagation modeling. In all likelihood, there are scenarios where ABFA's prediction methods break down. Because research in atmospheric acoustics has received rather modest funding during the past several decades, and the driving application has often been noise control rather than detection, there remain many scientific issues related to detection and signal coherence that need to be addressed by future research. Some of these follow:

1. *Calculation of mean sound levels in the presence of turbulent scattering.* It has been well documented that turbulent scattering substantially raises sound levels in refractive and topographic shadow regions (Gilbert, Raspet, and Di, 1990). At present, methods for incorporating realistic turbulent scattering into acoustical calculations are quite slow and impractical for use in a tool such as ABFA. Hence efficiency improvements in scattering calculations are much needed.
2. *Improvements to the scattered signal statistics.* The current version of ABFA does not properly account for the statistics of the scattered signal in the so-called "geometrical acoustics" regime, which is characterized by strong phase fluctuations and weak amplitude fluctuations. This situation occurs most often for low frequencies and short-to-moderate propagation distances. *Turbulent intermittency* (the tendency of turbulence to occur in bursts of activity) can also significantly affect detection (Wilson, 1996) and is unaccounted for at present.

3. *Improved calculation of the signal coherence.* The signal coherence model in ABFA assumes straight-line propagation. As a result, such potentially important effects as refraction and ground reflections are neglected in the coherence calculation. Future research on acoustic signal coherence, both experimental and theoretical, is needed.
4. *Decorrelation time of the acoustic signals.* ABFA estimates the time scale for decorrelation of the acoustic signal in a rather crude fashion from the friction velocity and height of the propagation path. This is necessary because so little information is available at present on the temporal decorrelation of acoustic signals.
5. *Reliance on structure-function parameters.* Structure-function parameters are convenient and accurate for describing the inertial subrange (small-scale) structure of turbulence. However, propagating acoustic waves are known also to be significantly affected by energy subrange (large-scale) turbulence structure. Research is under way at ARL to address this issue (Wilson, 1998a).
6. *Improved noise statistics.* Very little is known about the statistical distributions of noise in various environments, although this information is extremely important in probability-of-detection calculations. The limitations of the chi-squared distribution used by ABFA need to be ascertained.
7. *Wind noise models.* Wind noise plays a critical role in determining detection at low acoustic frequencies. The wind noise model currently used by ABFA is empirically based, and the limits of its applicability are not well known. Somewhat better, but still imperfect, models are available. It would be valuable to incorporate one of these other models into ABFA, or to develop a new, superior formulation for the wind noise.

References

Abramowitz, M., and I. A. Stegun (1965): *Handbook of Mathematical Functions*. Dover, San Francisco, pp 675–679.

Aki, K., and P. G. Richards (1980): *Quantitative Seismology*. W. H. Freeman, New York.

Attenborough, K., and O. Buser (1988): On the application of rigid-porous models to impedance data for snow. *J. Sound Vib.*, **124**, 315–327.

Bendat, J. S., and A. G. Piersol (1986): *Random Data: Analysis and Measurement Procedures*. Wiley-Interscience, New York.

Beranek, L. L. (1988): *Acoustical Measurements*. American Institute of Physics, Cambridge, MA.

Burdic, W. S. (1984): *Underwater Acoustic Signal Analysis*. Prentice-Hall, Englewood Cliffs, NJ.

Carl, D. M., T. C. Tarbell, and H. A. Panofsky (1973): Profiles of wind and temperature from towers over homogeneous terrain. *J. Atmos. Sci.*, **30**, 181–189.

Chien, C. F., and W. W. Soroka (1975): Sound propagation along an impedance plane. *J. Vib.*, **43**, 9–20.

Embleton, T.F.W., J. E. Piercy, and G. A. Daigle (1983): Effective flow resistivity of ground surfaces determined by acoustical measurements. *J. Acoust. Soc. Am.*, **74**, 1239–1244.

Flatté, S. M., R. Dashen, W. H. Munk, K. M. Watson, and F. Zachariasen (1979): *Sound Transmission through a Fluctuating Ocean*. Cambridge University Press, Cambridge.

Gilbert, K. E., R. Raspet, and X. Di (1990): Calculation of turbulence effects in an upward refracting atmosphere. *J. Acoust. Soc. Am.*, **87**, 2428–2437.

L'Espérance, A., J. Nicolas, D. K. Wilson, D. W. Thomson, Y. Gabillet, and G. Daigle (1993): Sound propagation in the atmospheric surface layer: Comparison of experiment with FFP predictions. *Appl. Acoust.*, **40**, 325–346.

Martens, M.J.M., L.A.M. van der Heijden, H.H.J. Walthaus, and W.J.J.M. van Rens (1985): Classification of soils based on acoustic impedance, air flow resistivity, and other physical soil parameters. *J. Acoust. Soc. Am.*, **78**, 970–980.

Noble, J. M. (1994): Evaluation of simple spherical spreading model for near vertical acoustical propagation. U.S. Army Research Laboratory, ARL-TR-532.

Panofsky, H. A., and J. A. Dutton (1984): *Atmospheric Turbulence: Models and Methods for Engineering Applications*. Wiley and Sons, New York.

Pierce, A. D. (1981): *Acoustics: An Introduction to Its Physical Principles and Applications*. McGraw-Hill, New York.

Raspet, R., S. W. Lee, E. Kuester, D. C. Chang, R. F. Richards, R. Gilbert, and N. Bong (1985): A fast-field program for sound propagation in a layered atmosphere above an impedance ground. *J. Acoust. Soc. Am.*, **77**, 345–352.

Song, B.-G., and J. A. Ritcey (1996): Angle of arrival estimation of plane waves propagating in random media. *J. Acoust. Soc. Am.*, **99**, 1370–1379.

Stull, R. B. (1988): *An Introduction to Boundary Layer Meteorology*. Kluwer, Dordrecht, Germany.

Tatarskii, V. I. (1971): *The Effects of the Turbulent Atmosphere on Wave Propagation*. Keter, Jerusalem.

Wilson, D. K. (1993): Sound field computations in a stratified, moving medium. *J. Acoust. Soc. Am.*, **94**, 400–407.

Wilson, D. K. (1996): The effect of turbulent intermittency on detection in acoustic shadows. U.S. Army Research Laboratory, ARL-TR-1002.

Wilson, D. K. (1997a): Performance of acoustic tracking arrays in atmospheric turbulence. U.S. Army Research Laboratory, ARL-TR-1286.

Wilson, D. K. (1997b): Simple, relaxational models for the acoustical properties of porous media. *Appl. Acoust.*, **50**, 171–188.

Wilson, D. K. (1998a): Anisotropic turbulence models for acoustic propagation through the neutral atmospheric surface layer. U.S. Army Research Laboratory, ARL-TR-1519.

Wilson, D. K. (1998b): Performance bounds for acoustic direction-of-arrival arrays operating in atmospheric turbulence. *J. Acoust. Soc. Am.*, **103**, 1306–1319.

Wilson, D. K., and D. W. Thomson (1994): Acoustic tomographic monitoring of the atmospheric surface layer. *J. Atmos. Ocean. Tech.*, **11**, 751–769.

Abbreviations and Acronyms

ABFA	Acoustic Battlefield Aid
ARL	Army Research Laboratory
CRLB	Cramer-Rao lower bound
FFP	fast field program
GUI	graphical user interface
MCF	mutual coherence function
MO	Monin-Obukhov
pdf	probability density function
rv	random variable
SNR	signal-to-noise ratio
TL	transmission loss

Distribution

Admnstr
Defns Techl Info Ctr
Attn DTIC-OCP
8725 John J Kingman Rd Ste 0944
FT Belvoir VA 22060-6218

Mil Asst for Env Sci
Ofc of the Undersec of Defns for Rsrch & Engrg R&AT E LS
Pentagon Rm 3D129
Washington DC 20301-3080

Ofc of the Dir Rsrch and Engrg
Attn R Menz
Pentagon Rm 3E1089
Washington DC 20301-3080

Ofc of the Secy of Defns
Attn ODDRE (R&AT) S Gontarek
The Pentagon
Washington DC 20301-3080

OSD
Attn OUSD(A&T)/ODDDR&E(R) R J Trew
Washington DC 20301-7100

AMCOM MRDEC
Attn AMSMI-RD W C McCorkle
Redstone Arsenal AL 35898-5240

ARL Chemical Biology Nuc Effects Div
Attn AMSRL-SL-CO
Aberdeen Proving Ground MD 21005-5423

Army Communications Elec Ctr for EW RSTA
Attn AMSEL-EW-D
FT Monmouth NJ 07703-5303

Army Corps of Engrs Engr Topographics Lab
Attn ETL-GS-LB
FT Belvoir VA 22060

Army Dugway Proving Ground
Attn STEDP 3
Attn STEDP-MT-DA-L-3
Attn STEDP-MT-M Bowers
Dugway UT 84022-5000

Army Field Artillery School
Attn ATSF-TSM-TA
FT Sill OK 73503-5000

Army Foreign Sci Tech Ctr
Attn CM
220 7th Stret NE
Charlottesville VA 22901-5396

Army Infantry
Attn ATSH-CD-CS-OR E Dutoit
FT Benning GA 30905-5090

Army Materiel Sys Analysis Activity
Attn AMXSY-AT Campbell
Attn AMXSY-CS Bradley
Aberdeen Proving Ground MD 21005-5071

Army Missile Cmnd
Attn AMSMI-RD-AC-AD Peterson
Redstone Arsenal AL 35898-5242

Army Missile Cmnd
Attn AMSMI-RD-DE-SE G Lill Jr
Redstone Arsenal AL 35898-5245

Army Missile Cmnd
Attn AMSMI-RD-AS-SS R Alongi
Redstone Arsenal AL 35898-5253

Army Rsrch Ofc
Attn AMXRO-GS Bach
PO Box 12211
Research Triangle Park NC 27709

Army Strat Defns Cmnd
Attn CSSD-SL-L Lilly
PO Box 1500
Huntsville AL 35807-3801

Army TACOM-ARDEC
Attn AMSTA-AR-WEL-TL
Bldg 59 Phillips Rd
Picatinny Arsenal NJ 07806-5000

CECOM
Attn PM GPS COL S Young
FT Monmouth NJ 07703

CECOM
Sp & Terrestrial Commctn Div
Attn AMSEL-RD-ST-MC-M H Soicher
FT Monmouth NJ 07703-5203

Distribution (cont'd)

Dir for MANPRINT
Ofc of the Deputy Chief of Staff for Prsnnl
Attn J Hiller
The Pentagon Rm 2C733
Washington DC 20301-0300

Hdqtrs Dept of the Army
Attn DAMO-FDT D Schmidt
400 Army Pentagon Rm 3C514
Washington DC 20301-0460

Hdqtrs Dept of the Army
Assist Secy of the Army for RD&A
Attn SARD-DOV H Fallin Rm 3E411
The Pentagon
Washington DC 20301-0103

Natl Security Agency
Attn W21 Longbothum
9800 Savage Rd
FT George G Meade MD 20755-6000

TACOM
Attn AMSTA-TR-R E Shalis
Mail Stop 263
Warren MI 48090

US Army ARDEC
Attn AMSTA-AR-FSF-RM J Heberley
Bldg 95N
Picatinny Arsenal NJ 07806

US Army CRREL
Attn CEREL-GP R Detsch
72 Lyme Rd
Hanover NH 03755-1290

US Army Edgewood RDEC
Attn SCBRD-TD J Vervier
Aberdeen Proving Ground MD 21010-5423

US Army Info Sys Engrg Cmnd
Attn ASQB-OTD F Jenia
FT Huachuca AZ 85613-5300

US Army Materiel Sys Analysis Activity
Attn AMXSY-CR Marchetti
Aberdeen Proving Ground MD 21005-5071

US Army Mis Cmnd (USAMICOM)
Attn AMSMI-RD-CS-R Documents
Redstone Arsenal AL 35898-5400

US Army Natick RDEC Acting Techl Dir
Attn SSCNC-T P Brandler
Natick MA 01760-5002

US Army Nuclear & Chem Agency
Attn MONA-ZB
Bldg 2073
Springfield VA 22150-3198

US Army OEC
Attn CSTE-EFS
Park Center IV 4501 Ford Ave
Alexandria VA 22302-1458

US Army Rsrch Ofc
Attn G Iafrate
4300 S Miami Blvd
Research Triangle Park NC 27709

US Army Simulation, Train, & Instrmntn Cmnd
Attn J Stahl
12350 Research Parkway
Orlando FL 32826-3726

US Army Tank-Automtv & Armaments Cmnd
Attn AMSTA-AR-TD C Spinelli
Bldg 1
Picatinny Arsenal NJ 07806-5000

US Army Tank-Automtv Cmnd Rsrch, Dev, & Engrg Ctr
Attn AMSTA-TA J Chapin
Warren MI 48397-5000

US Army Test & Eval Cmnd
Attn R G Pollard III
Aberdeen Proving Ground MD 21005-5055

US Army TRADOC Anlys Cmnd—WSMR
Attn ATRC-WSS-R
White Sands Missile Range NM 88002

US Army Train & Doctrine Cmnd
Battle Lab Integration & Techl Dirctrt
Attn ATCD-B J A Klevecz
FT Monroe VA 23651-5850

US Military Academy
Dept of Mathematical Sci
Attn MAJ D Engen
West Point NY 10996

Distribution (cont'd)

USATRADOC
Attn ATCD-FA
FT Monroe VA 23651-5170

Nav Air War Cen Wpn Div
Attn CMD 420000D C0245 A Shlanta
1 Admin Cir
China Lake CA 93555-6001

Nav Surface Warfare Ctr
Attn Code B07 J Pennella
17320 Dahlgren Rd Bldg 1470 Rm 1101
Dahlgren VA 22448-5100

Nav Surface Warfare Ctr
Attn Code G63
Dahlgren VA 22448-5000

Air Weather Service
Attn Techl Lib FL4414 3
Scott AFB IL 62225-5458

GPS Joint Prog Ofc Dir
Attn COL J Clay
2435 Vela Way Ste 1613
Los Angeles AFB CA 90245-5500

Hdqtrs AFWA/DNX
106 Peacekeeper Dr Ste 2N3
Offutt AFB NE 68113-4039

Phillips Laboratory
Attn PL/LYP Chisholm
Hanscom AFB MA 01731-5000

USAF Rome Lab Tech
Attn Corridor W Ste 262 RL SUL
26 Electr Pkwy Bldg 106
Griffiss AFB NY 13441-4514

USAFETAC DNE
Attn Glauber
Scott AFB IL 62225-5008

DARPA
Attn B Kaspar
3701 N Fairfax Dr
Arlington VA 22203-1714

University of Texas ARL Electromag Group
Attn Campus Mail Code F0250 A Tucker
Austin TX 78713-8029

Hicks & Associates Inc
Attn G Singley III
1710 Goodrich Dr Ste 1300
McLean VA 22102

US Army Rsrch Lab
Attn AMSRL-CI-LL Techl Lib (3 copies)
Attn AMSRL-CS-AL-TA Mail & Records Mgmt
Attn AMSRL-CS-EA-TP Techl Pub (3 copies)
Attn AMSRL-IS-E Battlefield Environ Div
Attn AMSRL-IS-EE D K Wilson (10 copies)
Attn AMSRL-SE-EE Z G Sztankay
Attn AMSRL-SE-SA J Eicke
Attn AMSRL-SE-SA N Srour
Attn AMSRL-SE-SA T Pham
Adelphi MD 20783-1197

REPORT DOCUMENTATION PAGE

Form Approved
OMB No. 0704-0188

1. AGENCY USE ONLY *(Leave blank)*	2. REPORT DATE	3. REPORT TYPE AND DATES COVERED
	September 1998	Final, January to December 1997

4. TITLE AND SUBTITLE

A Prototype Acoustic Battlefield Decision Aid Incorporating Atmospheric Effects and Arbitrary Sensor Layouts

5. FUNDING NUMBERS

DA PR: B53A
PE: 61102A

6. AUTHOR(S)

D. Keith Wilson

7. PERFORMING ORGANIZATION NAME(S) AND ADDRESS(ES)

U.S. Army Research Laboratory
Attn: AMSRL-IS-EE (dkwilson@arl.mil)
2800 Powder Mill Road
Adelphi, MD 20783-1197

8. PERFORMING ORGANIZATION REPORT NUMBER

ARL-TR-1708

9. SPONSORING/MONITORING AGENCY NAME(S) AND ADDRESS(ES)

U.S. Army Research Laboratory
2800 Powder Mill Road
Adelphi, MD 20783-1197

10. SPONSORING/MONITORING AGENCY REPORT NUMBER

11. SUPPLEMENTARY NOTES

AMS code: 61110253A11
ARL PR: 8FEJ60

12a. DISTRIBUTION/AVAILABILITY STATEMENT

Approved for public release; distribution unlimited.

12b. DISTRIBUTION CODE

13. ABSTRACT *(Maximum 200 words)*

The Acoustic Battlefield Aid (ABFA) is a prototype decision aid for assessing the performance of acoustic sensors in different environments. ABFA combines accurate modeling of atmospheric effects on acoustic signals with newly developed methods for determining acoustic array performance. The report describes the methods by which ABFA calculates such quantities as transmission loss, signal-to-noise ratio, detection probability, array direction-finding accuracy, and position-finding accuracy from array networks. Some example calculations are provided for propagation over rough terrain in various weather conditions.

14. SUBJECT TERMS

Acoustics, detection, atmosphere, decision aids

15. NUMBER OF PAGES

69

16. PRICE CODE

17. SECURITY CLASSIFICATION OF REPORT	18. SECURITY CLASSIFICATION OF THIS PAGE	19. SECURITY CLASSIFICATION OF ABSTRACT	20. LIMITATION OF ABSTRACT
Unclassified	Unclassified	Unclassified	UL

NSN 7540-01-280-5500

Standard Form 298 (Rev. 2-89)
Prescribed by ANSI Std. Z39-18
298-102

DEPARTMENT OF THE ARMY
U.S. Army Research Laboratory
2800 Powder Mill Road
Adelphi, MD 20783-1197